Inorg. Chem. **2004**, *43*, 4189–4202

Correlation of Structure and Function in Oligonuclear Zinc(II) Model Phosphatases

Bernhard Bauer-Siebenlist,[†] Franc Meyer,*[,†] Etelka Farkas,[‡] Denis Vidovic,[†] Jose Antonio Cuesta-Seijo,[†] Regine Herbst-Irmer,[†] and Hans Pritzkow[§]

Institut für Anorganische Chemie, Georg-August-Universität, Tammannstrasse 4, D-37077 Göttingen, Germany, Department of Inorganic and Analytical Chemistry, Faculty of Science, University of Debrecen, H-4010 Debrecen, Hungary, and Anorganisch-Chemisches Institut, Universität Heidelberg, Im Neuenheimer Feld 270, D-69120 Heidelberg, Germany

Received December 29, 2003

A series of pyrazolate-based dizinc(II) complexes has been synthesized and investigated as functional models for phosphoesterases, focusing on correlations between hydrolytic activity and molecular parameters of the bimetallic core. The Zn···Zn distance, the (bridging or nonbridging) position of the Zn-bound hydroxide nucleophile, and individual metal ion coordination numbers are controlled by the topology of the compartmental ligand scaffold. Species distributions of the various dizinc complexes in solution have been determined potentiometrically, and structures in the solid state have been elucidated by X-ray crystallography. The hydrolysis of bis(*p*-nitrophenyl)-phosphate (BNPP) promoted by the dinuclear phosphoesterase model complexes has been investigated in DMSO/buffered water (1:1) at 50 °C as a function of complex concentration, substrate concentration, and pH. Coordination of the phosphodiester has been followed by ESI mass spectrometry, and bidentate binding could be verified crystallographically in two cases. Drastic differences in hydrolytic activity are observed and can be attributed to molecular properties. A significant decrease of the pK_a of zinc-bound water is observed if the resulting hydroxide is involved in a strongly hydrogen-bonded intramolecular O_2H_3 bridge, which can be even more pronounced than for a bridging hydroxide. Irrespective of the pK_a of the Zn-bound water, a hydroxide in a bridging position evidently is a relatively poor nucleophile, while a nonbridging hydroxide position is more favorable for hydrolytic activity. Additionally, the metal array has to provide a sufficient number of coordination sites for activating both the substrate and the nucleophile, where phosphate diesters such as BNPP preferentially bind in a bidentate fashion, requiring a third site for water binding. Product inhibition of the active site by the liberated (*p*-nitrophenyl)phosphate is observed, and the product-inhibited complex could be characterized crystallographically. In that complex, the phosphate monoester is found to cap a rectangular array of four zinc ions composed of two bimetallic entities.

Introduction

Phosphodiesters that form the structural backbone of nucleic acids are extremely resistant to hydrolytic cleavage. The estimated half-life of RNA is 110 years, and that of DNA is in the range of 10−100 billion years.[1] As a consequence, nature has to use proper enzymes to accelerate the hydrolysis and to enable the processing of nucleic acids. Various of these phosphoesterases are known to contain two or even three cooperating zinc ions within their active site.[2−4] Being a strong Lewis acid with rapid ligand exchange and lacking any undesired redox activity, zinc is a preferred metal for catalyzing hydrolytic reactions.[5] Although different and specific mechanisms are probably involved for the individual

* Author to whom correspondence should be addressed. E-mail: franc.meyer@chemie.uni-goettingen.de.
[†] Georg-Universität Göttingen.
[‡] University of Debreen.
[§] Universität Heidelberg.

(1) Williams, N. H.; Takasaki, B.; Wall, M.; Chin, J. *Acc. Chem. Res.* **1999**, *32*, 485.
(2) Wilcox, D. E. *Chem. Rev.* **1996**, *96*, 2435.
(3) Sträter, N.; Lipscomb, W. N.; Klabunde, T.; Krebs, B. *Angew. Chem.* **1996**, *108*, 2159; *Angew. Chem., Int. Ed. Engl.* **1996**, *35*, 2024.
(4) Horton, N. C.; Perona, J. J. *Nat. Struct. Biol.* **2001**, *8*, 290.

10.1021/ic035491d CCC: $27.50
Published on Web 06/16/2004

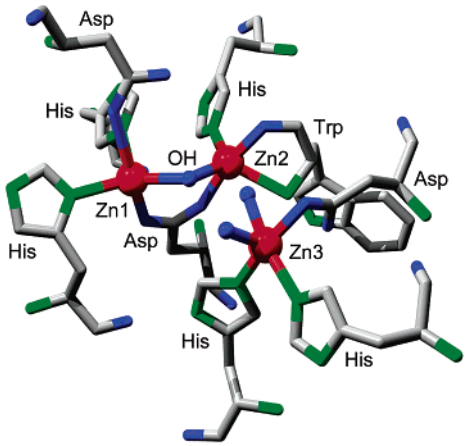

Figure 1. Trinuclear active site of P1 nuclease as determined by X-ray crystallography.[7]

Scheme 1. Proposed Mechanism of P1 Nuclease[7]

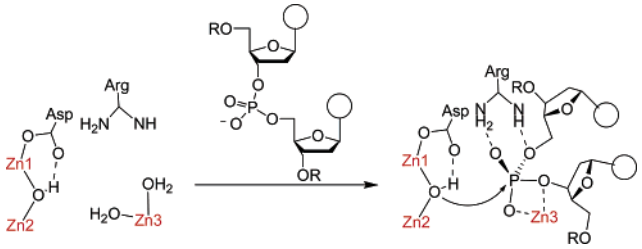

metalloenzymes, the general roles of the zinc ions are believed to include the generation of a hydroxide nucleophile at physiological pH by lowering the pK_a of water and the activation and orientation of the substrate through metal coordination as well as the stabilization of intermediates and of the oxyanion leaving group.[3,6]

An illustrative example is P1 nuclease, which cleaves single-stranded DNA and RNA into 5′-mononucleotides. It features a trinuclear zinc site (Figure 1; d(Zn1···Zn2) = 3.2 Å, d(Zn2···Zn3) = 4.7 Å), where a hydroxide bridging Zn1 and Zn2 is assumed to attack the phosphate substrate that bidentately binds to Zn3 (Scheme 1).[7] Despite manifold investigations, however, details of the mechanism of this and other metallohydrolases remain controversial. One crucial aspect under debate is the identity and the exact binding mode of the nucleophile.[8] A hydroxide (or water) spanning two zinc ions has been detected crystallographically in many hydrolases and is often considered as the active nucleophile, but it can be expected to exhibit rather low nucleophilicity if coordinated in a tightly bridging form. Thus, it has been suggested that, upon substrate binding, a shift of the bridging hydroxide to a terminal position occurs prior to attack on the coordinated substrate.[9]

Synthetic hydrolase models have been very useful in providing information on basic functional principles and mechanistic aspects of enzyme action. In addition, there is hope that artificial nucleases for biomimetic hydrolysis of DNA or RNA will eventually lead to beneficial applications in biotechnology and medicine.[10] As a consequence, considerable effort is directed toward the development of well-designed metal complexes that mediate the hydrolytic cleavage of DNA, RNA, or phosphodiester model substrates.[11−14] Despite the manifold studies, however, there still is only limited knowledge of the factors that govern hydrolytic activity of dizinc(II) arrays and a lack of general structure−reactivity correlations.[15−17]

In the present contribution, we report a comparative evaluation of the phosphodiesterase activity of a series of closely related, dinuclear zinc complexes, focusing on the binding mode of the hydroxide nucleophile and on the assessment of structural requirements for hydrolytic activity. Compartmental pyrazolate-based ligands are used as dinucleating scaffolds. As reported previously, a particular advantage of these ligands is the ability to fine-tune molecular characteristics of the bimetallic core, including the control of the metal−metal separation.[18−21] In addition, the pyrazolate is a reasonable compromise for mimicking carboxylate bridges that are widely found in nature but are difficult to incorporate into a polydentate compartmental ligand framework: just like a bridging carboxylate group,

(5) (a) Kimura, E.; Koike, T. *Adv. Inorg. Chem.* **1997**, *44*, 229. (b) Coleman, J. E. *Curr. Opin. Chem. Biol.* **1998**, *2*, 222.
(6) Cowan, J. A. *Chem. Rev.* **1998**, *98*, 1067.
(7) (a) Volbeda, A.; Lahm, A.; Sakiyama, F.; Suck, D. *EMBO J.* **1991**, *10*, 1607. (b) Romier, C.; Dominguez, R.; Lahm, A.; Dahl, O.; Suck, D. *Proteins* **1998**, *32*, 414.
(8) (a) Wang, Z.; Fast, W.; Benkovic, S. J. *Biochemistry* **1999**, *38*, 10013. (b) Zhan, C.-G.; Zheng, F. *J. Am. Chem. Soc.* **2001**, *123*, 2835.
(9) Bennett, B.; Holz, R. C. *J. Am. Chem. Soc.* **1997**, *119*, 1923.
(10) Hegg, E. L.; Burstyn, J. N. *Coord. Chem. Rev.* **1998**, *173*, 133.
(11) (a) Göbel, M. W. *Angew. Chem.* **1994**, *106*, 1201. (b) Krämer, R. *Coord. Chem. Rev.* **1999**, *182*, 243. (c) Blaskó, A.; Bruice, T. C. *Acc. Chem. Res.* **1999**, *32*, 475. (d) Molenveld, P.; Engbersen, J. F. J.; Reinhoudt, D. N. *Chem. Soc. Rev.* **2000**, *29*, 75. (e) Bashkin, J. K. *Curr. Opin. Chem. Biol.* **1999**, *3*, 752. (f) Rombach, M.; Maurer, C.; Weis, K.; Keller, E.; Vahrenkamp, H. *Chem. Eur. J.* **1999**, *5*, 1013. (g) Kimura, E. *Curr. Opin. Chem. Biol.* **2000**, *4*, 207. (h) Cowan, J. A. *Curr. Opin. Chem. Biol.* **2001**, *5*, 634.
(12) (a) Young, M. J.; Chin, J. *J. Am. Chem. Soc.* **1995**, *117*, 10577. (b) Cacciapaglia, R.; Di Stefano, S.; Kelderman, E.; Mandolini, L. *Angew. Chem.* **1999**, *111*, 359. (c) Jurek, P.; Martell, A. E. *Inorg. Chim. Acta* **1999**, *287*, 47. (d) Yamaguchi, K.; Akagi, F.; Fujinami, S.; Suzuki, M.; Shionoya, M.; Suzuki, S. *Chem. Commun.* **2001**, 375. (e) Gajda, T.; Düpre, Y.; Török, I.; Harmer, J.; Schweiger, A.; Sander, J.; Kuppert, D.; Hegetschweiler, K. *Inorg. Chem.* **2001**, *40*, 4918. (f) Sissi, C.; Rossi, P.; Felluga, F.; Formaggio, F.; Palumbo, M.; Tecilla, P.; Toniolo, C.; Scrimin, P. *J. Am. Chem. Soc.* **2001**, *123*, 3169. (g) Kühn, U.; Warzeska, S.; Pritzkow, H.; Krämer, R. *J. Am. Chem. Soc.* **2001**, *123*, 8125. (h) Fritsky, I. O.; Ott, R.; Pritzkow, H.; Krämer, R. *Chem. Eur. J.* **2001**, *7*, 1221. (i) Ichikawa, K.; Tarnai, M.; Uddin, M. K.; Nakata, K.; Sato, S. *J. Inorg. Biochem.* **2002**, *91*, 437. (j) Worm, K.; Chu, F.; Matsumoto, K.; Best, M. D.; Lynch, V.; Anslyn, E. V. *Chem. Eur. J.* **2003**, *9*, 741.
(13) (a) Kaminskaia, N. V.; He, C.; Lippard, S. J. *Inorg. Chem.* **2000**, *39*, 3365. (b) He, C.; Lippard, S. J. *J. Am. Chem. Soc.* **2000**, *122*, 184.
(14) Vichard, C.; Kaden, T. A. *Inorg. Chim. Acta* **2002**, *337*, 173.
(15) (a) Koike, T.; Kimura, E. *J. Am. Chem. Soc.* **1991**, *113*, 8935. (b) Chapman, W. H., Jr.; Breslow, R. *J. Am. Chem. Soc.* **1995**, *117*, 5462. (c) Iranzo, O.; Elmer, T.; Richard, J. P.; Morrow, J. R. *Inorg. Chem.* **2003**, *42*, 7737. (d) Zhu, L.; dos Santos, O.; Koo, C. W.; Rybstein, M.; Pape, L.; Canary, J. W. *Inorg. Chem.* **2003**, *42*, 7912.
(16) (a) Fujii, Y.; Itoh, T.; Onodera, K.; Tada, T. *Chem. Lett* **1995**, 305. (b) Itoh, T.; Fujii, Y.; Tada, T.; Yuzo, Y.; Hisada, H. *Bull. Chem. Soc. Jpn.* **1996**, *69*, 1265.
(17) Bonfá, L.; Gatos, M.; Mancin, F.; Tecilla, P.; Tonellato, U. *Inorg. Chem.* **2003**, *42*, 3943.
(18) Meyer, F.; Heinze, K.; Nuber, B.; Zsolnai, L. *J. Chem. Soc., Dalton Trans.* **1998**, 207.
(19) Meyer, F.; Rutsch, P. *Chem. Commun.* **1998**, 1037.
(20) (a) Meyer, F.; Kaifer, E.; Kircher, P.; Heinze, K.; Pritzkow, H. *Chem. Eur. J.* **1999**, *5*, 1617. (b) Ackermann, J.; Meyer, F.; Kaifer, E.; Pritzkow, H. *Chem. Eur. J.* **2002**, *8*, 247.
(21) Buchler, S.; Meyer, F.; Kaifer, E.; Pritzkow, H. *Inorg. Chim. Acta* **2002**, *337*, 371.

Chart 1. Ligands Used in the Present Work[21−23]

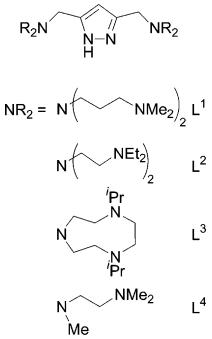

Chart 2. Complexes

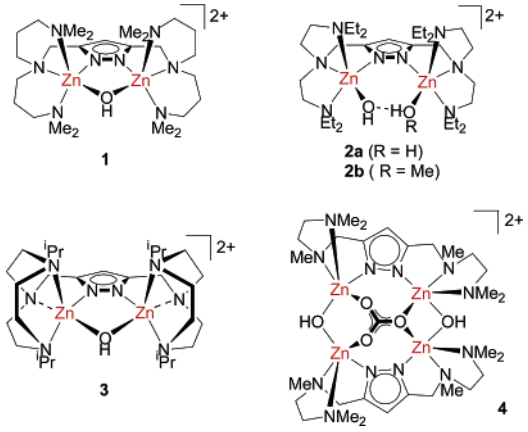

the pyrazolate provides a single negative charge, and it supports a similar range of metal−metal distances.[21] In this study we compare dizinc species with either a bridging hydroxide or an intramolecular O_2H_3 unit proposed to play a functional role in zinc hydrolases, and we contribute to the elucidation of structure−activity correlations of bio-inspired di- and oligozinc hydrolase mimics.

Structural Characterization of Complexes

A set of four pyrazolate-based dinucleating ligands, L^1−L^4, was employed in the present study (Chart 1). These ligands differ by (i) the chain lengths of the chelating side arms in the 3- and 5-positions of the heterocycle (L^1 versus L^2), (ii) the number of donor sites, i.e., the denticity of the coordination compartments (L^2 versus L^4), and (iii) ligand topology, i.e., macrocyclic versus open chain side arms (L^2 versus L^3).[21−23]

Dinuclear zinc(II) complexes of all ligands could be isolated and fully characterized (Chart 2), including solid-state X-ray crystal structures.[24] In all cases, the zinc ions are nested within the adjacent ligand compartments and are bridged by the pyrazolate, as anticipated. The length of the ligand side arms was previously shown to determine the metal−metal separation of the dinuclear scaffold.[18,19] In $[Zn_2L^1H_{-1}(OH)]^{2+}$ (**1**), the zinc ions may come rather close

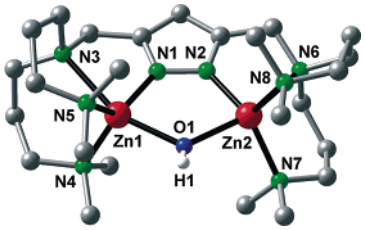

Figure 2. View of the molecular structure of **1**. In the interest of clarity, all protons except H1 have been omitted.[19]

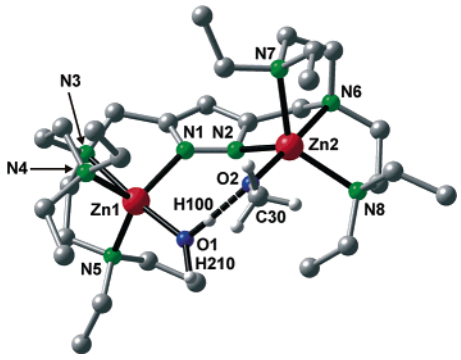

Figure 3. View of the molecular structure of **2b**. In the interest of clarity, all protons except those of the O_2H_2Me bridge have been omitted.

together (d(Zn···Zn) = 3.613 Å) and allow for a bridging position of a hydroxide coligand within the bimetallic pocket (Figure 2). In contrast, the shorter ligand side arms in **2a** and **2b** pull the two zinc ions back and apart, thus, enforcing much longer zinc−zinc distances. This prevents the small hydroxide from spanning the two metal ions and induces incorporation of an additional solvent molecule, water or MeOH, to give an O_2H_3 (**2a**) or O_2H_2Me (**2b**) bridging unit, respectively. The molecular structure of **2b** is depicted in Figure 3, and selected interatomic distances and angles are listed in Table 1. The metal ions are separated by more than 4 Å (d(Zn···Zn) = 4.406(1) [4.334(1)] Å) and are found in a roughly trigonal-bipyramidal coordination environment. The intermetallic distances in these complexes fall well within the range typically encountered in dinuclear zinc sites of natural hydrolases (e.g., P1 nuclease, d(Zn1···Zn2) = 3.2 Å and d(Zn2···Zn3) = 4.7 Å;[7] alkaline phosphatase, d(Zn···Zn) = 4.0 Å[25]). The O1···O2 distance of 2.436(4) [2.429(3)] Å in **2b** is indicative of a strong intramolecular hydrogen bond. Species **2a** and **2b** can be viewed as a solvated, resting form of a zinc-bound hydroxide next to an accessible coordination site at a proximate second zinc ion since the additional solvent molecule may easily be exchanged by, inter alia, substrate molecules. Consequently, **2a** gradually absorbs CO_2 from air to give a carbonato-bridged complex, while **1** does not, which is indicative of an enhanced reactivity of the masked terminal Zn−OH in **2a** and **2b** in comparison to the more tightly bound bridging hydroxide in **1**.[19]

Artificial nuclease activity and Zn-mediated hydrolytic reactions in a broader sense are best studied in buffered aqueous solution (or in media with high water content) in

(22) Meyer, F.; Beyreuther, S.; Heinze, K.; Zsolnai, L. *Chem. Ber./Recl.* **1997**, *130*, 605.
(23) Meyer, F.; Ruschewitz, U.; Schober, P.; Antelmann, B.; Zsolnai, L. *J. Chem. Soc., Dalton Trans.* **1998**, 1181.
(24) The structures of **2a** and **4**, as well as the structure of the BPh_4^- salt of **1**, have already been communicated.[19,26]
(25) Stec, B.; Holtz, K. M.; Kantrowitz, E. R. *J. Mol. Biol.* **2000**, *299*, 1323.

Table 1. Selected Interatomic Distances (Å) and Angles (deg) for **2b**[a]

Zn(1)−O(1)	1.982(3) [1.963(2)]
Zn(1)−N(1)	2.041(3) [2.046(3)]
Zn(1)−N(3)	2.280(3) [2.282(3)]
Zn(1)−N(4)	2.169(3) [2.190(3)]
Zn(1)−N(5)	2.135(3) [2.194(3)]
Zn(2)−O(2)	1.957(2) [1.958(3)]
Zn(2)−N2	2.067(3) [2.033(3)]
Zn(2)−N6	2.211(9) [2.343(14)] [2.269(3)]
Zn(2)−N7	2.261(8) [2.111(13)] [2.183(3)]
Zn(2)−N8	2.169(3) [2.148(3)]
O(2)−C(30)	1.359(6) [1.395(4)]
N(1)−N(2)	1.377(4) [1.382(4)]
Zn(1)···Zn(2)	4.406(1) [4.334(1)]
O1···O2	2.436(4) [2.429(3)]
N(1)−Zn(1)−O(1)	96.19(11) [99.22(10)]
N(1)−Zn(1)−N(4)	114.69(11) [120.52(10)]
O(1)−Zn(1)−N(4)	100.05(11) [99.86(10)]
N(1)−Zn(1)−N(5)	116.50(11) [111.53(10)]
O(1)−Zn(1)−N(5)	101.07(12) [100.49(10)]
N(4)−Zn(1)−N(5)	121.32(11) [119.31(10)]
N(1)−Zn(1)−N(3)	79.44(11) [79.13(10)]
O(1)−Zn(1)−N(3)	175.63(11) [178.29(9)]
N(4)−Zn(1)−N(3)	81.76(11) [80.66(10)]
N(5)−Zn(1)−N(3)	81.20(11) [80.61(10)]
N(2)−Zn(2)−O(2)	95.71(11) [100.84(11)]
N(2)−Zn(2)−N(7)	104.5(2) [104.2(3)] [109.81(11)]
O(2)−Zn(2)−N(7)	96.35(17) [112.3(3)] [98.46(11)]
N(2)−Zn(2)−N(8)	123.67(12) [111.91(10)]
O(2)−Zn(2)−N(8)	99.60(11) [97.35(11)]
N(7)−Zn(2)−N(8)	126.80(19) [118.6(3)] [131.28(11)]
N(2)−Zn(2)−N(6)	84.9(2) [75.1(3)] [81.17(10)]
O(2)−Zn(2)−N(6)	177.7(2) [166.9(3)] [177.97(11)]
N(7)−Zn(2)−N(6)	81.4(2) [79.5(4)] [81.01(10)]
N(8)−Zn(2)−N(6)	81.8(2) [78.6(3)] [81.61(10)]

[a] Values for the second (independent) molecule are shown in square brackets.

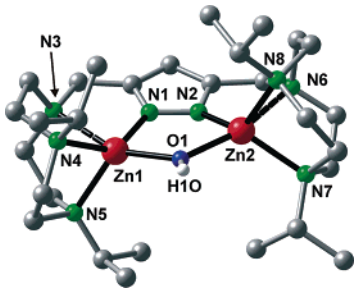

Figure 4. View of the molecular structure of **3**. In the interest of clarity, all protons except H1O have been omitted.

order to most closely mimic biological conditions. Hence, ligand L^3, bearing triazacyclononane-based side arms, was included in the present work. While related to L^2 (L^3 is topologically derived from L^2 by formally linking the outer N-donors), L^3 was expected to impart much higher stability to the resulting dizinc complexes in aqueous solution. Unexpectedly, however, a bridging hydroxide was found in the dizinc complex $[Zn_2L^3H_{-1}(OH)]^{2+}$ (**3**), despite the short ligand side arms that were assumed to induce a situation similar to **2a** (Figure 4; note that an O_2H_3 bridging unit was observed in a related dinickel(II) complex of L^3H_{-1}).[21] Closer inspection reveals that the short Zn···Zn separation in **3** (3.460(1) Å) is compensated by a significant elongation of the backside bonds between zinc and the bridgehead N (d(Zn1−N3) = 2.470(2) Å and d(Zn2−N6) = 2.401(2) Å), which gives rise to an overall {4 + 1} coordination of both

Table 2. Selected Interatomic Distances (Å) and Angles (deg) for **3**

Zn(1)−N(1)	1.955(2)	Zn(2)−O(1)	2.012(2)
Zn(1)−O(1)	2.000(2)	Zn(2)−N(7)	2.104(2)
Zn(1)−N(4)	2.104(2)	Zn(2)−N(8)	2.125(2)
Zn(1)−N(5)	2.137(2)	Zn(2)−N(6)	2.401(2)
Zn(1)−N(3)	2.470(2)	N(1)−N(2)	1.353(3)
Zn(2)−N(2)	1.965(2)	Zn(1)···Zn(2)	3.460(1)
N(1)−Zn(1)−O(1)	87.89(9)	N(2)−Zn(2)−N(7)	133.09(9)
N(1)−Zn(1)−N(4)	138.03(10)	O(1)−Zn(2)−N(7)	116.06(8)
O(1)−Zn(1)−N(4)	109.27(9)	N(2)−Zn(2)−N(8)	125.02(10)
N(1)−Zn(1)−N(5)	117.27(10)	O(1)−Zn(2)−N(8)	108.83(8)
O(1)−Zn(1)−N(5)	121.93(9)	N(7)−Zn(2)−N(8)	87.28(9)
N(4)−Zn(1)−N(5)	86.41(9)	N(2)−Zn(2)−N(6)	74.28(9)
N(1)−Zn(1)−N(3)	72.07(9)	O(1)−Zn(2)−N(6)	160.97(8)
O(1)−Zn(1)−N(3)	156.79(8)	N(7)−Zn(2)−N(6)	80.65(8)
N(4)−Zn(1)−N(3)	80.20(8)	N(8)−Zn(2)−N(6)	79.63(8)
N(5)−Zn(1)−N(3)	78.84(9)	Zn(1)−O(1)−Zn(2)	119.17(10)
N(2)−Zn(2)−O(1)	87.13(9)		

Zn ions. Consequently, the dinuclear scaffold in **3** appears to be somewhat strained, and it is likely that, in solution, the bridging hydroxide in **3** can more easily adopt a semibridging or even nonbridging position than the tightly bound hydroxide in **1**. Selected bond lengths and angles for **3** are listed in Table 2.

Ligand L^4 again provides short side arms but fewer donor sites than L^2. Its dizinc complexes thus allow for greater flexibility of the Zn_2 framework and offer additional coordination sites for substrate binding. Molecular models of $\{Zn_2L^4H_{-1}\}$ with the zinc ions in both tridentate coordination compartments suggest that the Zn···Zn distance is again unfavorable for an intramolecularly bridging hydroxide. Therefore, any Zn-bound water or hydroxide in $\{Zn_2L^4H_{-1}\}$ is quite reactive, and at neutral to basic pH, the dizinc complex of L^4H_{-1} was found to readily absorb CO_2 from air to give tetranuclear **4** (Chart 2). In **4**, two $\{Zn_2L^4H_{-1}\}$ subunits are linked by two hydroxide bridges, and the resulting rectangle of four zinc(II) ions is capped by a μ_4-carbonate.[26] For all phosphatase model studies described below, dinuclear species $\{Zn_2L^4H_{-1}\}$ (**4′**) were prepared in solution from L^4 and 2 equiv of $Zn(ClO_4)_2 \cdot 6H_2O$ and used without prior isolation of the complex.

To exclude any effects from different (and potentially coordinating) counteranions in the comparative reactivity studies, perchlorate salts of the complexes have been used in all cases.

Species in Solution

While the X-ray crystallographic results provide structural insights for the various complexes, the species distribution in solution is crucial for understanding any hydrolytic reactivity. Potentiometric titrations were performed to determine the pK_a values of the ligands (Table 3), as well as the stability constants of their zinc complexes and the pK_a values of zinc-bound water molecules in those complexes (Table 4). Values for L^2 and its zinc complexes have been reported previously.[27]

(26) Bauer-Siebenlist, B.; Meyer, F.; Vidovic, D.; Pritzkow, H. *Z. Anorg. Allg. Chem.* **2003**, *629*, 2152.
(27) Siegfried, L.; Kaden, T. A.; Meyer, F.; Kircher, P.; Pritzkow, H. *J. Chem. Soc., Dalton Trans.* **2001**, 2310.

Table 3. Protonation Constants of the Ligands at 25 °C ($I = 0.2$ M (KCl) for L^1, L^3, and L^4 and $I = 0.5$ M (KNO_3) for L^2)[a]

	L^1		$L^{2\,b}$		L^3		L^4	
species	$\log\beta$	pK_a	$\log\beta$	pK_a	$\log\beta$	pK_a	$\log\beta$	pK_a
$[LH_6]^{6+}$	46.61(4)	4.05						
$[LH_5]^{5+}$	42.55(2)	5.50			~9.35		~28	
$[LH_4]^{4+}$	37.05(3)	8.55	38.08(3)	8.58	8.82(1)	3.95	26.31(1)	3.53
$[LH_3]^{3+}$	28.50(1)	9.01	29.46(3)	9.34	4.87(1)	4.87	22.78(1)	4.96
$[LH_2]^{2+}$	19.49(1)	9.50	20.15(2)	9.76			17.82(1)	8.58
$[LH]^{+}$	9.99(2)	9.99	10.39(3)	10.39			9.24(1)	9.24

[a] Standard deviations of the values determined in this work are given in parentheses. [b] Reference 27.

Table 4. Complex Stability Constants with Zinc at 25 °C ($I = 0.2$ M (KCl) for L^1, L^3, and L^4; $I = 0.5$ M (KNO_3) for L^2)[a]

	$L^{2\,b}$		L^3		L^4	
species	$\log\beta$	pK_a	$\log\beta$	pK_a	$\log\beta$	pK_a
$[ZnLH_3]^{5+}$			7.41(6)		24.85(3)	4.66
$[ZnLH_2]^{4+}$	25.56(1)	8.07			20.19(3)	5.71
$[ZnLH]^{3+}$	17.49(3)	8.59			14.48(4)	
$[ZnL]^{2+}$	8.90(2)	9.87				
$[ZnLH_{-1}]^{+}$	−0.97(2)	11.31				
$[ZnLH_{-2}]$	−12.28(1)					
$[Zn_2LH]^{5+}$			1.24(4)	5.78	17.06(5)	6.58
$[Zn_2L]^{4+}$	<11.8		−4.54(6)	6.25	10.38(7)	6.53
$[Zn_2LH_{-1}]^{3+}$	4.78(3)	7.57	−10.79(5)	8.04	3.85(2)	7.66
$[Zn_2LH_{-2}]^{2+}$	−2.79(1)		−18.83(5)		−3.81(2)	

[a] Standard deviations of the values determined in this work are given in parentheses. [b] Reference 27.

Ligand Protonation Constants. The titrations were performed starting at acidic pH, using a potassium hydroxide titrant. From the titration curves, the deprotonation steps can be derived. In the case of L^4, four deprotonation steps could be found in the accessible pH range from 2 to 11.5. A further protonation/deprotonation step can be estimated to occur at a pH less than 2 but is just out of the detectable range. The exact locations of the deprotonations are very hard to differentiate, as the chemical settings of all four amine functions of L^4 are relatively equal. On the basis of chemical considerations, however, a dissociation/protonation sequence can be proposed. The first dissociation step (below pH 2) is assigned to the deprotonation of the very acidic, protonated pyrazole ring. In the following pair of steps, one proton is removed from each sidearm, and the final two deprotonations again correspond to the dissociation of one proton per sidearm. The difference in the pK_a values of $[L^4H_2]^{2+}$ and $[L^4H]^{+}$ of 0.66 is not much higher than the statistical value, which indicates highly independent deprotonation of the last two protons. This can most easily be explained by a sequence where each ethylenediamine sidearm accepts one proton. As a consequence, $[L^4H_4]^{4+}$ and $[L^4H_3]^{3+}$ also have to correspond to proton additions at different sides of the pyrazole unit. Hydrogen bonding with the pyrazole N might cause the pK_a of $[L^4H_3]^{3+}$ to be significantly higher than the pK_a of $[L^4H_4]^{4+}$ (the difference is 1.43 log units).

In the case of L^3, only two deprotonation steps could be clearly derived from the potentiometric results. These correspond to the removal of one proton per 1,4,7-triazacyclononyl (tacn) sidearm. Again, the very acidic pyrazole hydrochloride proton is out of range, i.e., below 2. The measurements indicate, however, that two further protons in $[L^3H_4]^{4+}$ are also quite acidic, most probably corresponding to one proton per tacn ring. This observation can be explained by the fact that the tacn ring would force two accumulated positive charges into close proximity. Hence, the release of a proton is thermodynamically favored, and the pK_a values are very low. The remaining two protons in $[L^3H_2]^{2+}$ — obviously one per macrocycle — are not removed up to pH 11, indicating very high pK_a values as a result of the "macrocyclic effect". The molecular structure of $[L^3H_2]^{2+}$, with one proton bound to each of the tacn side arms, could be confirmed by X-ray crystallography.[28] In line with these arguments, the pK_a values for $[L^2H_4]^{4+}$ and $[L^2H_3]^{3+}$ are significantly higher, and the pK_a values for $[L^2H_2]^{2+}$ and $[L^2H]^{+}$ are clearly lower than those of the corresponding L^3 species due to the open chain versus macrocyclic sidearm topologies. pK_a values for the L^1 system are quite similar to those of L^2, except for two additional protonation steps at $pK_a = 4.05$ and 5.50. Most probably, L^1 can take up a further proton in each sidearm at relatively high pH due to the larger separation of the protonation sites.

Species Distribution of Zinc Complexes. Titrations of the respective ligand in the presence of various equivalents of Zn^{2+} were analyzed in batch calculations, in which all titration curves are fitted at the same time with one model. Evaluation of the titration curves for Zn^{2+}/L^1 showed that this ligand has rather weak Zn^{2+}-chelating capabilities, as only the mononuclear species $[ZnL^1H_4]^{6+}$, $[ZnL^1H_3]^{5+}$, and $[ZnL^1H_2]^{4+}$ are formed in the region from pH 4 to 7. At higher pH, precipitation of zinc hydroxide was observed, and dinuclear species could not be calculated. This low affinity toward Zn^{2+} arises from the size of the chelate rings, where six-membered rings provide lower stability than five-membered chelate rings. In the case of L^4, the results of the fitting allowed the calculation of the stability constants of the mononuclear species $[ZnL^4H_3]^{5+}$, $[ZnL^4H_2]^{4+}$, and $[ZnL^4H]^{3+}$, as well as of the dinuclear species $[Zn_2L^4H]^{5+}$, $[Zn_2L^4]^{4+}$, $[Zn_2L^4H_{-1}]^{3+}$, and $[Zn_2L^4H_{-2}]^{2+}$. Calculations were restricted to a pH range between 2 and 8.5, as the precipitation of zinc hydroxide was observed at higher pH. Apparently, ligand L^4, with two tridentate coordination compartments, is not suited to efficiently bind two zinc ions in aqueous solutions in the basic pH region. $[Zn_2L^4H_{-1}]^{3+}$ and $[Zn_2L^4H_{-2}]^{2+}$ most probably are pyrazolate-bridged species, where the calculated pK_a value for $[Zn_2L^4H_{-1}]^{3+}$ of 7.66 thus marks the pK_a of metal-bound water to give a hydroxide function in $[Zn_2L^4H_{-2}]^{2+}$ (i.e., the stoichiometry of this species is better described as $[Zn_2L^4H_{-1}(OH)]^{2+}$). The pK_a of the related mononuclear system $[ZnL(OH_2)]^{2+}$ (L = diethylentriamine) is 8.93,[16] clearly indicating a significant increase in acidity due to the dinuclear arrangement.

In the case of L^3, the titration curves allowed the calculation of the stability constants for the mononuclear species $[ZnL^3H_3]^{5+}$ and the dinuclear species $[Zn_2L^3H]^{5+}$, $[Zn_2L^3]^{4+}$, $[Zn_2L^3H_{-1}]^{3+}$, and $[Zn_2L^3H_{-2}]^{2+}$ in the complete pH range from 2 to 10. No precipitation of zinc hydroxide occurs, and the formation of dinuclear complexes is found

(28) Buchler, S.; Meyer, F. Unpublished work.

at relatively low pH values, in accordance with the high stability of tacn-based complexes. In $[Zn_2L^3]^{4+}$, the two zinc ions presumably interact with the two tacn units, while the pyrazole remains uncoordinated. This species can be deprotonated to sequentially give the pyrazolate-bridged species $[Zn_2L^3H_{-1}]^{3+}$ and $[Zn_2L^3H_{-2}]^{2+}$, where the latter should correspond to complex **3**, characterized by X-ray crystallography in the solid state. The pK_a of 8.04 for $[Zn_2L^3H_{-1}]^{3+}$ thus signifies the pK_a of the zinc-bound water. This is lower than the pK_a of $[Zn(H_2O)_6]^{2+}$ (8.96)[29] and lower than most pK_a values of the zinc-bound water in five-coordinate, mononuclear zinc complexes with related tripodal ligands of the tris(aminoalkyl)amine) type ($[Zn(tren)(H_2O)]^{2+}$ pK_a = 10.68, $[Zn(Me_6tren)(H_2O)]^{2+}$ pK_a = 8.86, $[Zn(trpn)(H_2O)]$ pK_a = 9.99, $[Zn(Me_6trpn)(H_2O)]^{2+}$ pK_a = 8.01; tren = tris(2-aminoethyl)amine, Me_6tren = *N*′,*N*″,*N*‴-hexamethyl-tris(2-aminoethyl)amine, trpn = tris(3-aminopropyl)amine, Me_6trpn = *N*′,*N*″,*N*‴-hexamethyl-tris(3-aminopropyl)amine).[30] However, the pK_a of $[Zn_2L^3H_{-1}]^{3+}$ is still somewhat higher than expected if one considers that the hydroxide in **3** is located in a bridging position. Bridging water in dinuclear zinc(II) complexes is often found to have pK_a values below 8. On the other hand, the value of 8.04 for $[Zn_2L^3H_{-1}]^{3+}$ compares well with the pK_a of 8.15, determined for coordinated water in the dizinc complex of a related pyrazolate ligand bearing parent tacn side arms.[14] These relatively high pK_a values possibly reflect the strained situation within the bimetallic pocket of **3** and a semi- or nonbridging position of the zinc-bound water in solution (compare the discussion of the X-ray structural findings). $[Zn_2L^2H_{-2}]^{2+}$ is the only zinc complex of L^2 that is formed to any significant extent and most likely represents **2a**. The low pK_a value (7.57) for $[Zn_2L^2H_{-1}]^{3+}$ confirms the extra stabilization of the hydroxide in $[Zn_2L^2H_{-2}]^{2+}$ (**2a**) that results from its incorporation into the favorable O_2H_3 intramolecular bridge. It is interesting to note that involvement of the hydroxide in strong hydrogen-bonding (such as in the O_2H_3 bridge) can cause a more drastic decrease of the pK_a of Zn-bound water than incorporation of the resulting hydroxide in a potentially bridging position between two zinc ions. This once more emphasizes that a O_2H_3 unit might be a structural and possibly functional motif in oligozinc enzyme chemistry.[31,19]

Phosphate Diester Hydrolysis

Sodium bis(4-nitrophenyl)phosphate (NaBNPP) was used as a substrate in the present study. Cleavage of its phosphate ester bond and liberation of 4-nitrophenolate can be easily monitored by the strong absorption of the latter at 414 nm. Advantages and drawbacks of the use of the BNPP model substrate have been discussed in detail previously.[32]

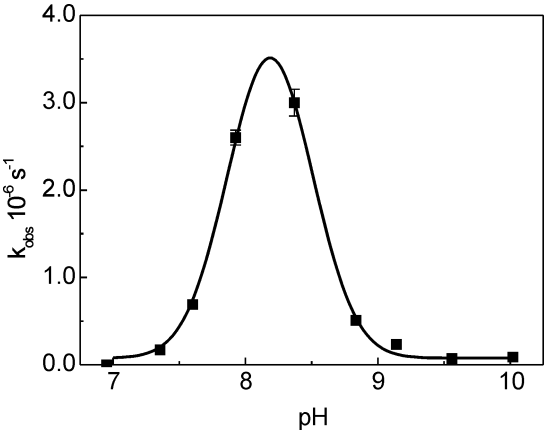

Figure 5. Effect of pH on BNPP hydrolysis mediated by **1**. $[\mathbf{1}]_0$ = 0.8 mM, $[BNPP]_0$ = 4 mM, at 50 °C, in DMSO/buffered H_2O (1:1).

A first screening of the hydrolytic activity of the various complexes was carried out at pH 8 in DMSO/buffered water (1:1) at 50 °C. While complex **2b** was used for the kinetic studies, the MeOH of the O_2H_2Me bridge will rapidly exchange with water in this solvent mixture to give the same species as **2a** in solution (the active species is denoted **2** in the following). Support for this assumption comes from ESI mass spectra of solutions of **2a** and **2b** in either methanol or water (see below). Rapid exchange of water and methanol ligands in the O_2H_2Me and O_2H_3 bridges had been confirmed earlier by stopped-flow studies on the corresponding dinickel(II) complexes (with $k_{obs} > 10^3$ s^{-1}).[33]

As described above, complex **1** is not stable at pH 8 in DMSO/buffered water (1:1). The pH-dependent pseudo-first-order rate constants for BNPP hydrolysis by **1** reveal a bell-shaped curvature due to the precipitation of $Zn(OH)_2$ at higher pH (Figure 5).

The kinetic data for **2**, **3**, and **4**′ show that the rate of hydrolysis of BNPP is linearly dependent on the complex concentration (Figure 6), in agreement with dinuclear active species in all cases. Pseudo-first-order constants, k_{obs} (defined by eq 1), are listed in Table 5 and follow the order **3** < **2** ≪

$$v_0 = k_{obs}[\text{complex}]_0 \qquad (1)$$

4′. The pH dependence of the initial rate was then measured and compared with the species distributions in order to identify the reactive species. For **3** and **4**′, plots of k_{obs} versus pH gave sigmoidal curves with inflection points that coincide with the pK_a values of the respective $[Zn_2LH_{-1}]$ complexes (Figures 7 and 8), clearly indicating that $[Zn_2LH_{-2}]$ must be the active species and that a Zn-bound hydroxide is required for hydrolytic activity (a slight shift in the curves for **3** may result from the different solvent systems used for speciation and kinetic studies, i.e., water versus DMSO/water 1:1). At pH > 8.5 the activity of **4**′ drops rapidly due to the instability of this complex under basic conditions.

(29) Gade, L. H. *Koordinationschemie*; Wiley-VCH: Weinheim, Germany, 1998; p 436.
(30) (a) Coates, J. H.; Gentle, G. J.; Lincoln, S. F. *Nature* **1974**, *249*, 773. (b) Canary, J. W.; Xu, J.; Castagnetto, J. M.; Rentzeperis, D.; Marky, L. A. *J. Am. Chem. Soc.* **1995**, *117*, 11545. (c) Ibrahim, M. M.; Ichikawa, K.; Shiro, M. *Inorg. Chim. Acta* **2003**, *353*, 187.
(31) Ruf, M.; Weis, K.; Vahrenkamp, H. *J. Am. Chem. Soc.* **1996**, *118*, 9288.
(32) Menger, F. M.; Ladika, M. *J. Am. Chem. Soc.* **1987**, *109*, 3145.
(33) Kryatov, S. V.; Rybak-Akimova, E. V.; Meyer, F.; Pritzkow, H. *Eur. J. Inorg. Chem.* **2003**, 1581.

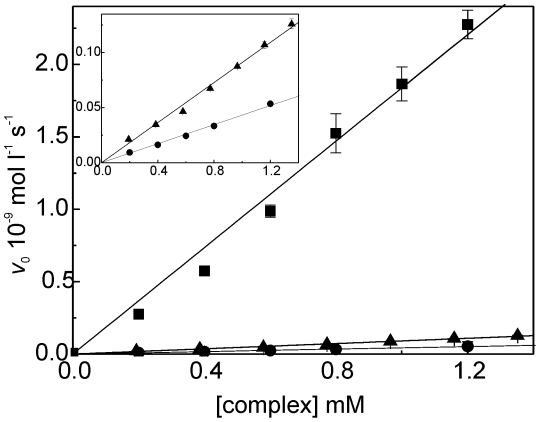

Figure 6. Initial rate vs complex concentration for BNPP hydrolysis promoted by **2** (▲), **3** (●), and **4′** (■); $[BNPP]_0 = 2$ mM, at 50 °C, pH = 8.28, in DMSO/HEPES buffer (1:1).

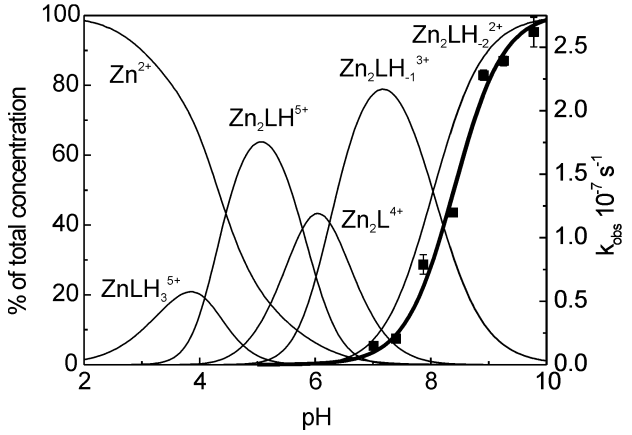

Figure 7. Species distribution and pH/rate profile for BNPP hydrolysis promoted by **3**; $[\mathbf{3}]_0 = 0.8$ mM, $[BNPP]_0 = 4$ mM, in DMSO/buffered H_2O (1:1).

Table 5. Kinetic Data for BNPP Hydrolysis Promoted by Zinc(II) Complexes at 50 °C and pH 8.28 in DMSO/Buffered Water (1:1)

complex	k_{obs} (s^{-1})[a]	k_{cat} (s^{-1})	K_M (mM)
2	$(9.1 \pm 0.2) \times 10^{-8}$	$(1.9 \pm 0.3) \times 10^{-6}$	42 ± 4
3	$(4.3 \pm 0.1) \times 10^{-8}$		
4′	$(1.8 \pm 0.1) \times 10^{-6}$	$(4.2 \pm 0.2) \times 10^{-5}$	55 ± 1

[a] Experimental conditions given in Figure 6.

In contrast, Figure 9 reveals that, in the case of **2**, the species $[Zn_2L^2H_{-2}]$, which is assumed to represent the O_2H_3-bridged complex **2a**, is not reactive. Above pH 7.5, where $[Zn_2L^2H_{-2}]$ starts to become predominant, the rate of BNPP hydrolysis decreases. The (relatively low) activity of the $\{Zn_xL^2\}$ system (**2**) is apparently caused by minor mono- and dinuclear species that exist around pH 8.

Table 6 compares the reactivity of the present complexes with those of $Zn(ClO_4)_2$ (i.e., with "free" Zn^{2+} ions) at pH 7.4, which is the maximum possible pH for such comparison since precipitation of $Zn(OH)_2$ at pH > 7.5 is observed in the case of $Zn(ClO_4)_2$ (while complexes **3** and **4′** become considerably more active at higher pH, see above). From the data it is obvious that the different activities of **2**, **3**, and **4′** do not simply reflect the number of accessible free coordination sites. In particular, **4′** is much more active than

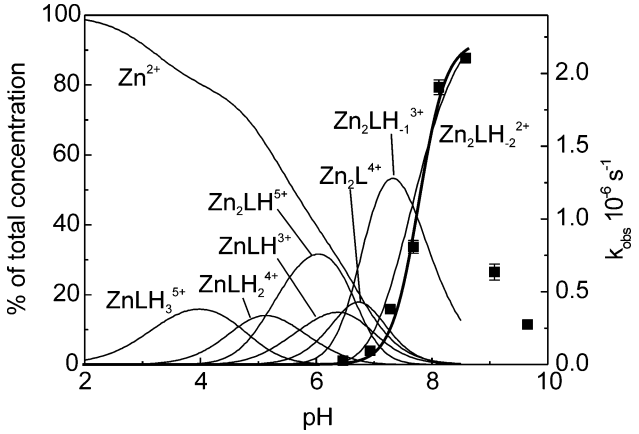

Figure 8. Species distribution and pH/rate profile for BNPP hydrolysis promoted by **4′**; $[L^4]_0 = 0.8$ mM, $[Zn^{2+}]_0 = 1.6$ mM, $[BNPP]_0 = 2$ mM, in DMSO/buffered H_2O (1:1).

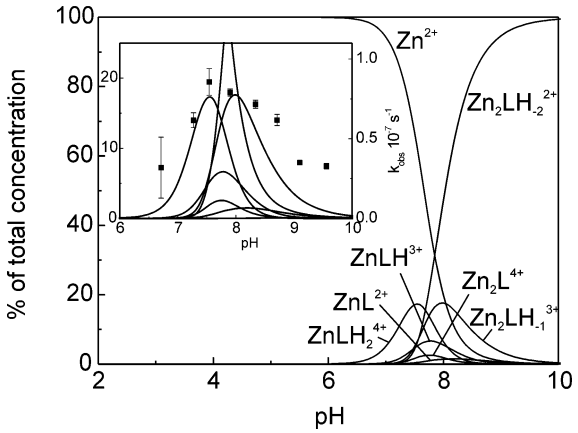

Figure 9. Species distribution of the complexes of L^2 with 2 equiv of Zn^{2+} ($ZnLH_{-1}^{+}$ species are formed at low concentrations). The inset shows an overlay of the species distribution and the pH/rate profile for BNPP hydrolysis promoted by **2**; $[\mathbf{2b}]_0 = 0.8$ mM, $[BNPP]_0 = 2$ mM, in DMSO/buffered H_2O (1:1).

Table 6. Rate Constants k_{obs} for BNPP Hydrolysis Promoted by Dinuclear Zinc(II) Complexes and $Zn(ClO_4)_2$ at 50 °C and pH 7.4 in DMSO/Buffered Water (1:1)[a]

complex	k_{obs} (s^{-1})[a]	$[BNPP]_0$ (mM)
2	$(8.6 \pm 0.8) \times 10^{-8}$	2
3	$(2.2 \pm 0.3) \times 10^{-8}$	4
4′	$(38.1 \pm 0.5) \times 10^{-8}$	2
$Zn(ClO_4)_2$	$(4.5 \pm 0.3) \times 10^{-8}$	2

[a] $[Complex]_0$ is 0.8 mM for 2, 3, 4′; $[Zn^{2+}]_0$ is 1.6 mM for $Zn(ClO_4)_2$.

"free" Zn^{2+}, even at pH 7.4, clearly indicating some promoting effect due to cooperativity of the proximate metal ions.

The dependence of the initial rate of hydrolysis on substrate concentration (Figures 10−12) shows that the reaction is first order in BNPP for **3** — and also for **2** and **4′** if the latter are present at low concentrations. At higher BNPP concentrations, however, a diminution of the reaction rate for **2** and **4′** (Figures 10 and 12) indicates saturation behavior, which can be explained by the substrate binding preequilibrium illustrated in Scheme 2. Such a feature is reminiscent of Michaelis−Menten behavior, typical for native metalloenzymes. Kinetic data for **2** and **4′** have been modeled by

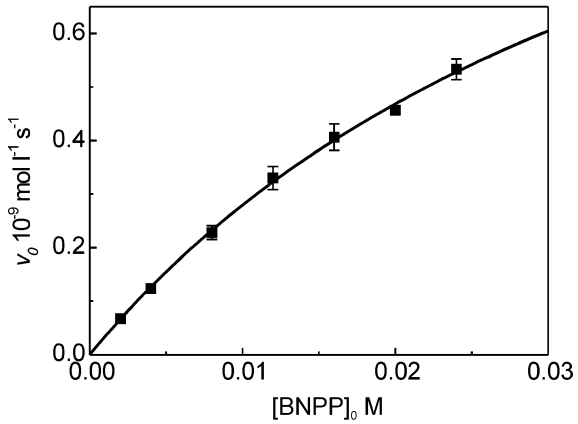

Figure 10. Effect of BNPP concentration on the initial rate of its hydrolysis mediated by **2**; [**2b**]$_0$ = 0.8 mM, pH = 8.28, in DMSO/HEPES buffer (1:1).

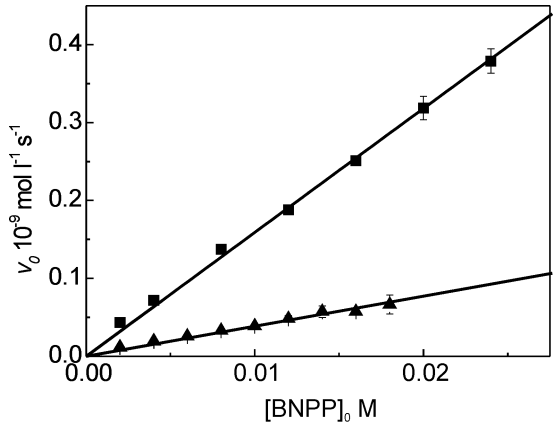

Figure 11. Effect of BNPP concentration on the initial rate of its hydrolysis mediated by **3**; [**3**]$_0$ = 0.8 mM (■); [**3**]$_0$ = 0.2 mM (▲), pH = 8.28, in DMSO/HEPES buffer (1:1).

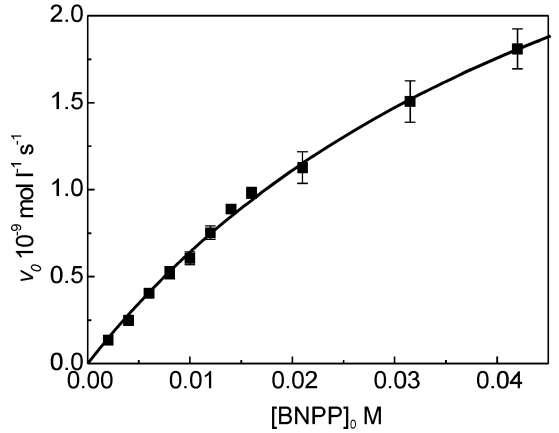

Figure 12. Effect of BNPP concentration on the initial rate of its hydrolysis mediated by **4′**; [L^4]$_0$ = 0.1 mM, [Zn^{2+}]$_0$ = 0.2 mM, pH = 8.28, in DMSO/HEPES buffer (1:1).

the rate law given in eq 2 to yield values for K_M and k_{cat}, as listed in Table 5.

$$v_0 = \frac{k_{cat}[\text{complex}]_0[\text{BNPP}]_0}{K_M + [\text{BNPP}]_0} \quad \text{with} \quad K_M = \frac{k_{-1} + k_{cat}}{k_1} \qquad (2)$$

Evidently, the substrate binding constants $K = k_1/k_{-1} = 1/K_M$ of 24 ± 3 M^{-1} (for **2**) and 18 ± 1 M^{-1} (for **4′**) are quite low,[34] in accordance with earlier observations that BNPP is a weak ligand.[13,14] The absence of any saturation effects for **3**—even at a large excess of the substrate—suggests either direct attack of the Zn-bound hydroxide on BNPP (without prior coordination of the substrate) or an even lower substrate binding constant.

Scheme 2

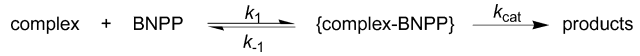

Table 7. Second-Order Rate Constants for BNPP Hydrolysis Promoted by Zinc(II) Complexes at 50 °C and pH 8.28 in DMSO/Buffered Water (1:1)

complex	k_{app} ($M^{-1}s^{-1}$)	k_{bim} ($M^{-1}s^{-1}$)	pK_a of Zn-bound water
2	$(4.5 \pm 0.2) \times 10^{-5}$		7.57
3	$(2.1 \pm 0.2) \times 10^{-5}$	$(3.3 \pm 0.3) \times 10^{-5}$	8.04
4′	$(9.0 \pm 0.5) \times 10^{-4}$	$(1.1 \pm 0.1) \times 10^{-3}$	7.66

The apparent second-order rate constants (k_{app}) for all systems are listed in Table 7. Assuming that [$Zn_2L^3H_{-2}$] and [$Zn_2L^4H_{-2}$] are the only active species in the case of **3** and **4′**, the true second-order constants (k_{bim}) can be obtained by dividing k_{app} by the percentage factor deduced from the species distribution at the respective pH (eq 3).

$$v_0 = k_{app}[\text{complex}]_0[\text{BNPP}]_0 = k_{bim}[Zn_2LH_{-2}][\text{BNPP}]_0 \qquad (3)$$

Binding of Phosphate Diesters

The binding of BNPP to the various zinc complexes has been studied by ESI mass spectrometry and ^{31}P NMR spectroscopy in solution. In addition, the binding of the hydrolytically more inert dimethyl phosphate (DMP) has been investigated since, in this case, any ester cleavage can be definitely excluded on the NMR and MS time scales.

ESI Mass Spectrometry. In the ESI mass spectra of methanol solutions of **2a** or **2b**, the ion [Zn_2L^2(OMe)-(ClO_4)]$^+$, containing a simple OMe bridge, is observed, and spectra of water solutions will give a dominant peak for [Zn_2L^2(OH)(ClO_4)]$^+$. This is in accordance with rapid exchange and facile extrusion of the additional solvent molecule in the original O_2H_3 or O_2H_2Me units.

After addition of 1 equiv of NaBNPP to a methanol solution of each complex, the respective ESI spectra reveal[35] a dominant peak for the starting complex devoid of one of the perchlorate counterions, as well as further species with bound BNPP. Only in the case of **1** is a major peak for the free ligand [L^{1}H]$^+$ detected, confirming the much lower stability of this system in solution. Association of BNPP occurs via the displacement of ClO_4^- in the case of **1**, **3**, and **4** to give [$Zn_2L^1H_{-1}$(OH)(BNPP)]$^+$, [$Zn_2L^3H_{-1}$(OH)-(BNPP)]$^+$, and [Zn_4(L$^4H_{-1}$)$_2$(CO_3)(OH)$_2$ (BNPP)]$^+$, respectively, but it occurs via complete substitution of the O_2H_2Me bridge in the case of **2b** to give [$Zn_2L^2H_{-1}$(BNPP)(ClO_4)]$^+$. This clearly indicates that the O_2H_2Me (or O_2H_3) group in

(34) Assuming $k_{cat} \ll k_{-1}$.
(35) Only major peaks are discussed; see Supporting Information for a list of major peaks in tabular form.

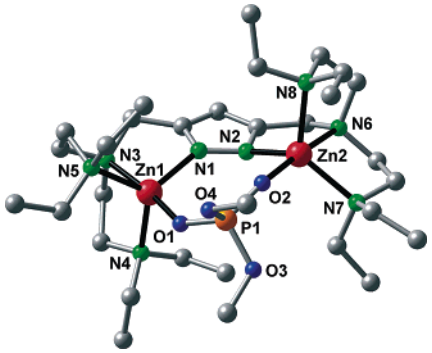

Figure 13. View of the molecular structure of **5b**. In the interest of clarity, all hydrogen atoms have been omitted.

the latter complex is quite labile, whereas the bridging hydroxide in **1** and **3** is more tightly bound. To labilize the Zn−OH−Zn function and to mimic more acidic pH conditions, a second set of ESI-MS experiments was conducted in the presence of 1 equiv of $HClO_4$. Any protonation and release of the metal-bound hydroxide was anticipated to facilitate the binding of BNPP, and this is confirmed by the larger relative intensity of the peaks corresponding to the BNPP-bound species under these conditions. Furthermore, in the presence of acid, the BNPP substrate preferentially replaces the metal-bound hydroxide instead of a perchlorate: e.g., for complex **3**, besides the parent ion $[Zn_2L^3H_{-1}(OH)(ClO)_4]^+$, the species $[Zn_2L^3H_{-1}(BNPP)(ClO_4)]^+$ is now found under acidic conditions. In the case of **4**, addition of $HClO_4$ causes the tetranuclear compound to fall apart, leading to dinuclear species with one or two BNPP molecules coordinated.

According to ESI mass spectrometry, DMP binds to the zinc complexes more strongly than BNPP, giving rise to species with one or two DMP ligands associated—the latter situation being the most dominant in all cases but **2b**. In contrast to **1** and **3**, no species that retain an OMe (or OH) group are detected for **2b**, suggesting that the labile moiety in the bimetallic pocket of **2b** is completely replaced by the DMP ligand.

To verify bidentate, bridging coordination of DMP to the $\{Zn_2L^2H_{-1}\}$ scaffold with replacement of the intramolecular O_2H_3/O_2H_2Me unit in **2a**/**2b**, the complex $[Zn_2L^2H_{-1}(DMP)](ClO_4)_2$ (**5b**−$(ClO_4)_2$) has been synthesized independently and characterized by X-ray crystallography (Figure 13).

In complex **5b**, the $(MeO)_2PO_2^-$ substrate analogue is coordinated in the expected fashion within the clamp of the two zinc ions (d(Zn1···Zn2) = 4.406(1) [4.365(1)] Å; two independent but similar molecules are found per asymmetric unit). The structure resembles those of the dizinc cores, with bound phosphate diester substrate, proposed for many metallohydrolases. Interestingly, the zinc ions in **5b** are severely displaced out of the plane of the pyrazolate heterocycle (by 0.567−0.794 [0.580−0.616] Å). Although all bond lengths are in the usual range, this displacement may indicate a somewhat strained binding situation. Considering the similarity of the $[Zn_2L^2H_{-1}(BNPP)(ClO_4)]^+$ and $[Zn_2L^2H_{-1}(DMP)(ClO_4)]^+$ species in the ESI spectra discussed above, the crystallographic structure of **5b** is assumed to provide a good model for the binding of the BNPP substrate in **5a** (Scheme 3).

Table 8. Selected Interatomic Distances (Å) and Angles (deg) for **5b**[a]

Zn1−N1	2.047(2) [2.035(2)]
Zn1−N3	2.221(2) [2.207(2), 2.32(2)]
Zn1−N4	2.151(2) [2.138(3), 2.21(1)]
Zn1−N5	2.164(2) [2.153(4), 2.15(2)]
Zn1−O1	1.993(2) [1.997(2)]
Zn2−N2	2.047(2) [2.043(2)]
Zn2−N6	2.242(2) [2.233(2)]
Zn2−N7	2.134(2) [2.157(2)]
Zn2−N8	2.141(2) [2.159(2)]
Zn2−O2	2.012(2) [1.980(2)]
O2−P1	1.490(2) [1.490(2)]
O1−P1	1.493(2) [1.487(2)]
P1−O4	1.587(2) [1.583(2)]
P1−O3	1.577(2) [1.579(2)]
N1−N2	1.381(2) [1.377(2)]
Zn1···Zn2	4.406(1) [4.365(1)]
O(1)−Zn(1)−N(1)	106.52(7) [100.83(7)]
O(1)−Zn(1)−N(4)	98.06(6) [92.55(8), 107.5(3)]
N(1)−Zn(1)−N(4)	108.39(7) [117.03(8), 104.0(3)]
O(1)−Zn(1)−N(5)	91.02(6) [99.72(9), 94.6(4)]
N(1)−Zn(1)−N(5)	125.13(7) [116.3(1), 121.1(5)]
N(4)−Zn(1)−N(5)	120.24(7) [121.4(1),124.5(6)]
O(1)−Zn(1)−N(3)	171.63(6) [176.17(8), 172.7(3)]
N(1)−Zn(1)−N(3)	80.97(7) [79.91(8), 80.8(3)]
N(4)−Zn(1)−N(3)	82.75(7) [83.80(9), 78.8(4)]
N(5)−Zn(1)−N(3)	81.45(6) [83.2(1), 78.6(5)]
O(2)−Zn(2)−N(2)	98.55(6) [106.87(7)]
O(2)−Zn(2)−N(7)	96.26(7) [92.47(6)]
N(2)−Zn(2)−N(7)	127.63(7) [125.61(7)]
O(2)−Zn(2)−N(8)	100.28(7) [96.69(6)]
N(2)−Zn(2)−N(8)	104.70(7) [100.80(7)]
N(7)−Zn(2)−N(8)	121.50(7) [127.36(7)]
O(2)−Zn(2)−N(6)	176.17(7) [171.48(6)]
N(2)−Zn(2)−N(6)	80.67(7) [81.56(7)]
N(7)−Zn(2)−N(6)	81.37(7) [81.29(7)]
N(8)−Zn(2)−N(6)	83.53(7) [82.69(7)]
O(2)−P(1)−O(1)	118.96(8) [118.38(9)]
O(2)−P(1)−O(3)	106.32(8) [105.45(8)]
O(1)−P(1)−O(3)	110.36(8) [110.41(9)]
O(2)−P(1)−O(4)	110.20(8) [110.07(8)]
O(1)−P(1)−O(4)	104.78(8) [106.24(9)]
O(3)−P(1)−O(4)	105.48(8) [105.65(8)]

[a] Values for the second (independent) molecule are shown in square brackets.

Scheme 3. Binding of Phosphate Diesters by **2a**.

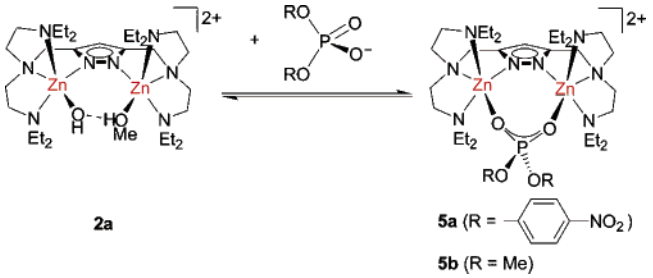

Phosphate binding similar to the case of **5a** can also be predicted for **4′**, where the ligand side arms have the same chain lengths. This is confirmed by the isolation and X-ray crystallographic characterization of $[Zn_2L^4H_{-1}(DMP)(NO_3)_2]$ (**6**), in which the phosphate binds in the expected bidentate fashion to the dizinc unit (Figure 14). Due to the fewer donor sites in L^4 compared to L^2, the remaining coordination sites have to be occupied by additional ligands, such as the two nitrates in **6**. Each of these nitrates binds in a bidentate

Table 9. Selected Interatomic Distances (Å) and Angles (deg) for **6**

Zn(1)−O(1)	2.009(3)	Zn(2)−N(2)	2.058(3)
Zn(1)−N(1)	2.056(4)	Zn(2)−N(4)	2.159(4)
Zn(1)−N(6)	2.131(4)	Zn(2)−O(5)	2.215(3)
Zn(1)−O(10)	2.227(3)	Zn(2)−N(3)	2.254(3)
Zn(1)−O(8)	2.261(3)	Zn(2)−O(7)	2.291(3)
Zn(1)−N(5)	2.306(3)	N(2)−N(1)	1.362(5)
Zn(2)−O(2)	1.995(3)	Zn1···Zn2	4.307(2)
O(1)−Zn(1)−N(1)	105.37(13)	O(2)−Zn(2)−O(5)	88.21(13)
O(1)−Zn(1)−N(6)	97.17(13)	N(2)−Zn(2)−O(5)	102.61(13)
N(1)−Zn(1)−N(6)	105.85(14)	N(4)−Zn(2)−O(5)	150.28(13)
O(1)−Zn(1)−O(10)	93.70(12)	O(2)−Zn(2)−N(3)	173.79(13)
N(1)−Zn(1)−O(10)	95.97(13)	N(2)−Zn(2)−N(3)	79.64(13)
N(6)−Zn(1)−O(10)	151.96(14)	N(4)−Zn(2)−N(3)	82.93(13)
O(1)−Zn(1)−O(8)	87.83(12)	O(5)−Zn(2)−N(3)	88.62(12)
N(1)−Zn(1)−O(8)	152.00(12)	O(2)−Zn(2)−O(7)	85.47(12)
N(6)−Zn(1)−O(8)	96.60(13)	N(2)−Zn(2)−O(7)	157.43(13)
O(10)−Zn(1)−O(8)	57.98(11)	N(4)−Zn(2)−O(7)	93.48(12)
O(1)−Zn(1)−N(5)	176.86(14)	O(5)−Zn(2)−O(7)	57.70(11)
N(1)−Zn(1)−N(5)	77.77(13)	N(3)−Zn(2)−O(7)	88.33(12)
N(6)−Zn(1)−N(5)	81.94(13)	O(2)−P(1)−O(1)	118.84(18)
O(10)−Zn(1)−N(5)	85.80(12)	O(2)−P(1)−O(4)	105.07(19)
O(8)−Zn(1)−N(5)	89.28(12)	O(1)−P(1)−O(4)	110.20(18)
O(2)−Zn(2)−N(2)	106.27(13)	O(2)−P(1)−O(3)	111.07(19)
O(2)−Zn(2)−N(4)	97.26(14)	O(1)−P(1)−O(3)	105.98(18)
N(2)−Zn(2)−N(4)	103.79(13)	O(4)−P(1)−O(3)	104.90(17)

chelating mode to one of the zinc ions with two relatively long Zn−O bonds [d(Zn−O) = 2.215(3)−2.291(3) Å]. The metals are thus found in a distorted octahedral environment. If more weakly coordinating counterions such as ClO_4^- are present instead of the nitrates, it is likely that solvent molecules fill up the *exo* coordination sites at the zinc ions. In particular, water should be bound in aqueous solution.

^{31}P NMR Spectroscopy. Titrations of the dizinc complexes **2a** and **3** with phosphates have been followed by ^{31}P NMR spectroscopy in order to quantitatively probe the binding of phosphate diesters to the dizinc complexes as an important factor of substrate activation. Instead of BNPP, the hydrolytically more stable DMP was used to avoid any cleavage on the time scale of the NMR experiment. Aliquots of dimethylphosphoric acid were added consecutively to the dizinc complexes **2a** and **3** in a buffered water/DMSO mixture at pH 8. The complexes bind DMP rapidly, inducing a high-field shift of the ^{31}P NMR signal of about 4 ppm. Addition of an excess of dimethylphosphoric acid shows that only 1 equiv of phosphate coordinates to the complex. Analysis of the titrations curves according to the equilibrium reaction 1 gives binding constants $K_B = (9.3 \pm 4.4) \times 10^3$ M^{-1} for **2a** and $(2.7 \pm 0.9) \times 10^3$ M^{-1} for **3**. The higher binding constant for **2a** reflects the greater stability of the OH bridge in **3** compared to the O_2H_3 bridge in **2a**. It may also indicate that the longer Zn···Zn distance is better suited to accommodate the phosphate in a O,O′-bridging mode.

$$[Zn_2LH_{-2}] + DMP \overset{K_B}{\rightleftharpoons} [Zn_2LH_{-1}(DMP)] \qquad (4)$$

Product Inhibition of the Active Site

To evaluate whether the most active complex **4′** acts as a catalyst for the cleavage of BNPP, the reaction was followed by ^{31}P NMR spectroscopy. Figure 15 reveals a quickly decreasing reaction rate and a turnover that levels off at less than 0.5 equiv of the substrate. While the reason for the

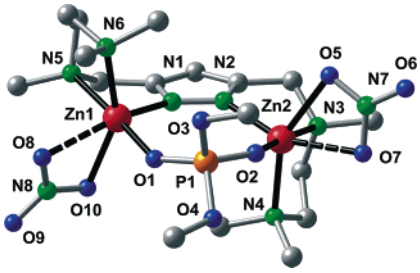

Figure 14. View of the molecular structure of **6**. In the interest of clarity, all hydrogen atoms have been omitted.

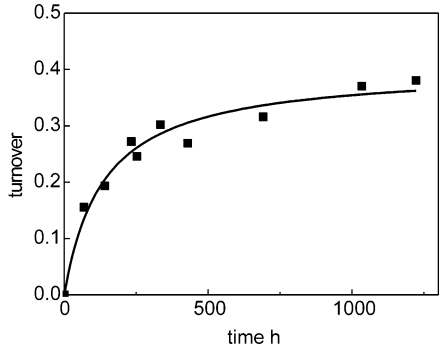

Figure 15. Hydrolysis of BNPP by **4′**, followed by ^{31}P NMR; pH 8.28, at 50 °C, in DMSO/buffered H_2O (1:1).

Scheme 4. Formation of the Product-Inhibited Complex **7**.

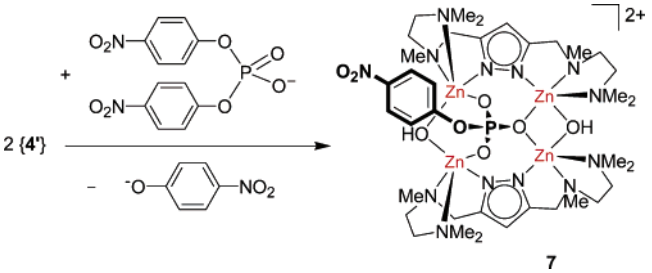

stoichiometry of less than 0.5 is unclear, one might assume formation of some inactive, carbonate-bridged $[Zn_4L^4(OH)_2(CO_3)]^{2+}$ (**4**; see above) through the absorption of aerial CO_2 under the reaction conditions. The noncatalytic behavior of **4′** indicates efficient product inhibition of the active site, where each 4-nitrophenyl phosphate (NPP) formed upon cleavage of BNPP blocks more than one $\{Zn_2L^4H_{-2}\}$ species. No further hydrolysis of NPP to give free phosphate could be detected by ^{31}P NMR spectroscopy. Single crystals of the product-inhibited complex **7** (Scheme 4) could be obtained directly from the reaction mixture and were characterized by X-ray diffraction. The molecular structure of **7** is depicted in Figure 16, together with selected atom distances and bond angles that are listed in Table 10.

In **7**, two $\{Zn_2L^4H_{-1}\}$ moieties are linked by two hydroxide bridges to constitute a tetranuclear array of four zinc ions that is capped by a μ_4-η^2:η^1:η^1 bridging NPP. **7** can thus be described as two $[Zn_2L^4H_{-2}]$ species inhibited by a single product molecule from the BNPP hydrolysis. The NPP blocks all four coordination sites at the metal ions, and further hydroxide nucleophilicity in **7** is diminished because of its tight bridging mode. ESI mass spectrometry shows that the tetranuclear species **7** is also present in solution. Product inhibition is a general phenomenon in phosphate diester

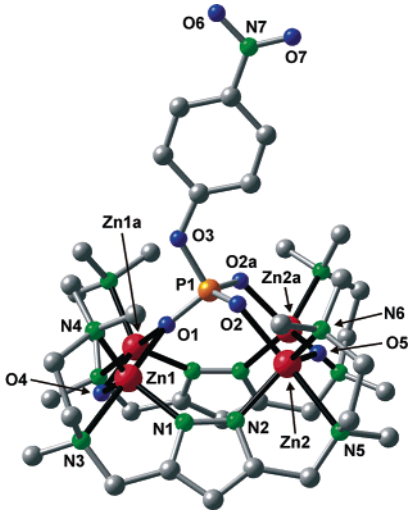

Figure 16. View of the molecular structure of **7**. In the interest of clarity, all hydrogen atoms have been omitted.

Table 10. Selected Interatomic Distances (Å) and Angles (deg) for **7**

P(1)−O(1)	1.505(8)	Zn(1)−N(3)	2.279(7)
P(1)−O(2)	1.510(5)	Zn(2)−O(5)	1.957(4)
P(1)−O(3)	1.641(10)	Zn(2)−N(2)	2.049(6)
O(1)−Zn(1)	2.122(5)	Zn(2)−N(6)	2.131(7)
O(2)−Zn(2)	2.061(6)	Zn(2)−N(5)	2.338(7)
Zn(1)−O(4)	1.985(6)	Zn1···Zn1a	3.146(2)
Zn(1)−N(1)	2.021(7)	Zn1···Zn2	4.257(2)
Zn(1)−N(4)	2.111(8)	Zn2···Zn2a	3.545(2)

Zn(1a)−O(1)−Zn(1)	95.7(3)	O(5)−Zn(2)−O(2)	96.9(3)
Zn(2)−O(5)−Zn(2a)	129.8(5)	N(2)−Zn(2)−O(2)	98.2(2)
Zn(1)−O(4)−Zn(1a)	104.8(4)	O(5)−Zn(2)−N(6)	119.8(3)
O(4)−Zn(1)−N(1)	118.9(4)	N(2)−Zn(2)−N(6)	118.3(3)
O(4)−Zn(1)−N(4)	126.5(4)	O(2)−Zn(2)−N(6)	88.8(3)
N(1)−Zn(1)−N(4)	112.9(3)	O(5)−Zn(2)−N(5)	96.0(3)
O(4)−Zn(1)−O(1)	79.7(3)	N(2)−Zn(2)−N(5)	78.7(3)
N(1)−Zn(1)−O(1)	103.9(3)	O(2)−Zn(2)−N(5)	166.4(2)
N(4)−Zn(1)−O(1)	100.4(3)	N(6)−Zn(2)−N(5)	81.2(3)
O(4)−Zn(1)−N(3)	93.3(3)	O(1)−P(1)−O(2)	112.5(3)
N(1)−Zn(1)−N(3)	79.2(3)	O(2)−P(1)−O(2a)	116.1(4)
N(4)−Zn(1)−N(3)	83.8(3)	O(1)−P(1)−O(3)	100.0(4)
O(1)−Zn(1)−N(3)	173.0(3)	O(2)−P(1)−O(3)	107.0(3)
O(5)−Zn(2)−N(2)	120.0(3)		

hydrolysis by biomimetic complexes and is reminiscent of metalloenzyme behavior. The present study represents a rare case where the product-inhibited metal species could be clearly identified and fully characterized.

Discussion

Since a decrease of the pK_a of metal-bound water can generally be expected to bring about a decrease of the nucleophilicity of the resulting hydroxide,[16] a reactivity order **3** > **4′** > **2** would have been anticipated from simply looking at the relative pK_a values, which is clearly reverse to the experimentally observed order at pH 8.28 (compare Table 7). More subtle effects taking into account the individual complex constitution have to be considered. In particular, the difference in activity **3** ≪ **4′** allows some conclusions with respect to the efficiency of the Zn-bound hydroxide in its different binding modes: a more tightly bound hydroxide in a bridging position as observed in the least active **3** seems to be unfavorable because of its diminished nucleophilicity, irrespective of the pK_a. Since the masked, terminal hydroxide in **2a** was then anticipated to exhibit significantly enhanced nucleophilicity, however, other effects have to play a decisive role as well and have to be responsible for the negligible activity of **2a** (residual activity is mainly due to several other $\{Zn_xL^2\}$ species, collectively denoted as **2**, see Figure 9). On the basis of the DMP binding studies, the ESI-MS experiments, and the structure of **5b** described above, it can be assumed that the BNPP substrate binds to **2a** in a bidentate fashion within the bimetallic pocket (Scheme 3), with complete replacement of the O_2H_3 unit. While this might lead to some activation of the substrate, all coordination sites in the resulting **5a** are now blocked, and activation of water to give a nucleophilic Zn-bound hydroxide is no longer possible. Although a reaction path that proceeds via six-coordinate zinc ions cannot be fully excluded, there has been no indication so far that expanded coordination of zinc(II) ions in $\{Zn_2L^2H_{-1}\}$ complexes is feasible. Ample precedence exists for five-coordinate zinc(II) complexes of tripodal, tetradentate ligands, such as tren or Me_6tren, and it is well established that zinc complexes of Me_6tren cannot form six-coordinate complexes[36] (L^2 can be viewed as two coupled Me_5tren-type donor compartments[27,37]). It should also be noted that the O_2H_3 bridging moiety in the related dinickel(II) complex $[Ni_2L^2H_{-1}(O_2H_3)]^{2+}$ was previously shown to act as a base rather than as a nucleophile toward some potentially bridging substrates, such as urea, yielding stable bidentate incorporation of anionic ureate.[33,38] Consequently, $[Zn_2L^2H_{-2}]$ (**2a**) itself is hydrolytically inactive toward bidentate substrates, such as BNPP. The low residual activity of the $\{Zn_xL^2\}$ system at medium pH can be traced to the presence of different minor species (**2**) in solution, as is evidenced by the overlay of the pH/rate profile and species distribution shown in Figure 9.

In contrast, in the case of **3**, the zinc-bound hydroxide in the species $[Zn_2L^3H_{-2}]$ is not replaced by the incoming BNPP and is clearly responsible for hydrolytic cleavage of the substrate. Nevertheless, the activity of **3** is low, which we assume to have two causes. First, the binding constant for coordination of the substrate is very low, which can be attributed to the shielding of the metal ions by the nonlabile and bulky tacn side arms and the lack of easily accessible coordination sites at the dizinc core. Second, the bridging hydroxide in **3** is more tightly bound within the clamp of the two zinc ions and exhibits low nucleophilicity. On the basis of the structural findings discussed above, it is tempting to suggest that, upon substrate binding, the hydroxide shifts toward a semibridging or even nonbridging position and thereby gains at least some nucleophilic character.

The X-ray crystallographic results for **5b** and **6** suggest a similar bidentate substrate binding for both **2** and **4′**, in accordance with the very similar K_M values that result from the Michaelis−Menten analyses of the two systems. The major advantage of **4′** is the availability of additional

(36) (a) Di Vaira, M.; Orioli, P. L. *Acta Crystallogr. B* **1968**, *24*, 1269. (b) Lincoln, S. F.; Hounslow, A. M.; Coates, J. H. *Inorg. Chim. Acta* **1983**, *77*, L7. (c) Xu, X.; Lajmi, A. R.; Canary, J. W. *Chem. Commun.* **1998**, 2701. (d) Ibrahim, M. M.; Ichikawa, K.; Shiro, M. *Inorg. Chem. Commun.* **2003**, *6*, 1030.

coordination sites at the metal ions. These support bidentate substrate binding and, at the same time, allow for the generation of an active Zn-bound hydroxide nucleophile from water, which cannot be trapped in an intramolecularly bridging position like in **3** but still is in close proximity to the bound substrate. Hence, $[Zn_2L^4H_{-2}]$ is identified as the active species and a 20-fold higher k_{cat} value compared to that of **2** is observed. Taken together, the second-order rate constants for **4′** are around 20−30 times larger than those for either **2** or **3**, but this has distinct causes in each case, as explained above. Clear-cut comparison with results for related mononuclear systems reported in the literature is hampered by the widely differing reaction conditions used in such studies.[39] Some representative apparent second-order rate constants for BNPP hydrolysis by zinc(II) complexes with mononucleating ligands L are the following: $k = 1.1 \times 10^{-5}$ M^{-1} s^{-1} (L = tren, in water, $I = 0.1$ M NaCl, at 25 °C), $k = 9.7 \times 10^{-5}$ M^{-1} s^{-1} (L = 1,3,5-triaminocyclohexane, in water, $I = 0.1$ M NaCl, at 25 °C), and $k = 0.39 \times 10^{-5}$ M^{-1} s^{-1} (L = [12]aneN$_4$, in water, $I = 0.1$ M NaCl, at 25 °C).[17]

Conclusions

Several points relevant to biological phosphoesterase action and to the design of biomimetic hydrolases can be inferred from this work: (i) Involvement in strong hydrogen bonding (such as in the O_2H_3 bridge) can cause an even more drastic decrease of the pK_a of Zn-bound water than incorporation of the resulting hydroxide in a bridging position between two zinc ions, thus corroborating that O_2H_3 units might play a functional role in oligozinc hydrolases.[19,31] A more tightly fixed hydroxide in the clamp of two metal ions should be a relatively poor nucleophile, while a nonbridging hydroxide appears to be more favorable for hydrolytic activity. However, such a nonbridging position of the zinc-bound hydroxide is not sufficient alone, as revealed by the low activity of $[Zn_2L^2H_{-2}]$ (**2a**). (ii) The metal array has to provide a sufficient number of coordination sites for activating both the substrate *and* the nucleophile. In the case of phosphate diesters such as BNPP, the substrate preferentially binds in a bidentate fashion (as is supported by the X-ray crystal structures of **5b** and **6**), requiring a further third site for water binding. This may be achieved either by a trinuclear center (such as in P1 nuclease, Scheme 1) or by a high degree of coordinative unsaturation of a bimetallic array, such as in **4′**. However, comparison with the activity of $Zn(ClO_4)_2$ (i.e., "free" Zn^{2+}, see Table 6) clearly reveals that the differences in activity for the present series of complexes do not merely reflect the blocking of essential free sites. A promoting effect due to cooperative action of the proximate zinc ions is apparent, in particular for the most active compound **4′**. (iii) Since a phosphate monoester usually is a better ligand than a diester, product inhibition remains a latent problem in bioinspired systems. In the case of **7**, this leads to aggregation and inactivation of the catalytic site. Low binding constants and high lability of the phosphates (both substrate and product) toward the active site are therefore necessary to enable multiple turnover, which makes a high reactivity to the nucleophile (i.e., high k_{cat} values) even more important for achieving acceptable reaction rates.

Experimental Section

General. When necessary, reactions and manipulations were carried out under an atmosphere of nitrogen by using standard Schlenk techniques in order to avoid CO_2 contamination. Solvents were dried by established processes. HPLC grade methanol (CHROMASOLV) was obtained from Riedel-de-Haen. Ligands L^1, L^2, L^3, and L^4 and complex **4** were synthesized according to the reported methods.[21−23,26] All other chemicals were purchased from commercial sources and used as received. Microanalyses were performed by the Analytisches Labor des Instituts für Anorganische Chemie der Universität Göttingen, UV-vis spectra were recorded with an Analytik Jena Specord 100, IR spectra (as KBr pellets) with a Digilab Excalibur, FAB-MS spectra with a Finnigan MAT 95, and ESI-MS spectra with a Finnigan MAT LCQ. NMR spectra were recorded with Bruker Avance 500, Avance 300, and Avance 200, measured at 300 K. The solvent signal was used as the chemical shift reference (d_6-acetone $\delta_H = 2.04$, $\delta_C = 29.8$; d_6-DMSO $\delta_H = 2.49$, $\delta_C = 39.7$). ^{31}P spectra were externally referenced to 85% phosphorous acid.

Caution! Although no problems were encountered in this work, transition metal perchlorate complexes are potentially explosive and should be handled with proper precautions.

Synthesis of $[Zn_2L^1H_{-1}(OH)](ClO_4)_2$ (1). A solution of L^1 (629 mg, 1.35 mmol) in MeOH (150 mL) was treated with 2 equiv of KO*t*Bu (303 mg) and 2 equiv of $Zn(ClO_4)_2 \cdot 6H_2O$ (1004 mg) and stirred at room temperature for 12 h. All volatile material was then evaporated under reduced pressure, the residue taken up in acetone (70 mL) and filtered, and the solution was layered with light petroleum to gradually yield colorless crystals (592 mg, 54%) of the product **1**. The synthesis and X-ray crystallographic characterization of the BPh_4^- salt of **1** has been communicated previously.[19] ^{1}H NMR (500 MHz, d_6-acetone, 27 °C) $\delta = 6.09$ (s, 1H, pz-H^4), 3.76 (s, 4H, pz-CH$_2$), 3.29 (br, 4H, CH$_2$), 2.80 (br, 36H, CH$_2$, CH$_3$), 2.55 (br, 8H, CH$_2$), 2.15 (br, 8H, CH$_2$). ^{13}C NMR (126 MHz, d_6-acetone, 27 °C) $\delta = 150.3$ (pz-C^{3,5}), 100.1(pz-C^4), 62.6, 54.8, 54.0, 50.8, 48.4, 23.0. MS (ESI) 709.5 (100, $[Zn_2L^1H_{-1}(OH)(ClO_4)]^+$). IR (KBr) 3614 (m), 3115 (w), 2932 (br, m), 2851 (m), 1712 (m), 1465 (m), 1183 (m), 1098 (vs), 1014 (m), 973 (m), 804 (m), 623 (s). Elemental analysis calcd (%) for $C_{25}H_{54}N_8Cl_2O_9Zn_2$ (812.4) C 36.96 H 6.70 N 13.79; found C 36.94 H 6.79 N 12.55.

Synthesis of $[Zn_2L^2H_{-1}(MeOH)(OH)](ClO_4)_2$ (2b). A solution of L^2 (300 mg, 0.57 mmol) in MeOH (70 mL) was treated with 2 equiv of KO*t*Bu (129 mg) and 2 equiv of $Zn(ClO_4)_2 \cdot 6H_2O$ (427 mg) and stirred at room temperature for 12 h. All volatile material was then evaporated under reduced pressure, the residue taken up in methanol (50 mL) and filtered, and the solution layered with diethyl ether to gradually yield colorless crystals (401 mg, 75%) of the product **2b**. ^{1}H NMR (500 MHz, d_6-DMSO, 27 °C) $\delta =$ 5.93 (s, 1H, pz-H^4), 3.86 (s, 4H, CH$_2$), 2.77−2.67 (m, br, 32H, CH$_2$), 1.01 (s, br, 24H, CH$_3$). ^{13}C NMR (500 MHz, d_6-DMSO, 27 °C) $\delta = 151.1$ (pz-C^{3,5}), 97.1 (pz-C^4), 53.1, 51.1, 50.9, 50.0, 46.6, 11.5, 8.9. IR (KBr) 2979 (s), 2944 (s), 2881 (s), 1473 (s), 1386 (m), 1263 (m), 1096 (vs), 983 (m), 736 (m), 623 (s). MS (ESI) 779.4 (60, $[Zn_2L^2H_{-1}(OMe)(ClO_4)]^+$), 765.5 (20, $[Zn_2L^2H_{-1}(OH)$-

(37) (a) Röder, J. C.; Meyer, F.; Pritzkow, H. *Organometallics* **2001**, *20*, 811. (b) Röder, J. C.; Meyer, F.; Winter, R. F.; Kaifer, E. *J. Organomet. Chem.* **2002**, *641*, 113.
(38) Meyer, F.; Pritzkow, H. *Chem. Commun.* **1998**, 1555.
(39) Ibrahim, M. M.; Shimomura, N.; Ichikawa, K.; Shiro, M. *Inorg. Chim. Acta* **2001**, *313*, 125.

$(ClO_4)]^+$). Elemental analysis calcd (%) for $C_{30}H_{66}Cl_2N_8O_{10}Zn_2 \cdot CH_3OH$ (932.6) C 39.92, H 7.57, N 12.02; found C 39.77, H 7.56, N 12.20.

Synthesis of $[Zn_2L^3H_{-1}(OH)](ClO_4)_2$ (3). A solution of L^3 (428 mg, 0.83 mmol) in MeOH (100 mL) was treated with 2 equiv of KO*t*Bu (185 mg) and 2 equiv of $Zn(ClO_4)_2 \cdot 6\ H_2O$ (614 mg) and stirred at room temperature for 12 h. All volatile material was then evaporated under reduced pressure, the residue taken up in acetone (50 mL) and filtered, and the solution layered with light petroleum to gradually yield colorless crystals (571 mg, 80%) of the product **3**. ^{1}H NMR (200 MHz, d_6-acetone, 27 °C) δ = 6.02 (s, 1H, pz-H^4), 4.11 (s, 4H, CH_2), 3.64 (sept, $^3J_{HH}$ = 6.6 Hz, 4H, CH), 3.13 (m, 16H, CH_2), 2.81 (m, 8H, CH_2), 1.17 (d, $^3J_{HH}$ = 6.6 Hz, 24H, CH_3). ^{13}C NMR (75 MHz, d_6-acetone, 27 °C) δ = 148.5 (pz-C^{3,5}), 99.4 (pz-C^4), 58.1, 55.7, 53.0, 52.0, 22.9, 16.1. IR (KBr) 2969 (s), 2931 (m), 2873 (m), 1998 (w), 1694 (m), 1489 (m), 1370 (m), 1285 (m), 1088 (vs), 622 (s). MS (FAB) 762 (80, $[Zn_2L^3H_{-1}(OH)(ClO_4)]^+$). Elemental analysis calcd (%) for $C_{29}H_{58}Cl_2N_8O_9Zn_2$ (864.5) C 40.29, H 6.76, N 12.96; found C 40.16, H 6.73, N 12.41.

Synthesis of $[Zn_2L^2H_{-1}\{O_2P(OMe)_2\}](ClO_4)_2$ (5b). A solution of L^2 (140 mg, 0.27 mmol) in MeOH (50 mL) was treated with 2 equiv of KO*t*Bu (60 mg), 2 equiv of $Zn(ClO_4)_2 \cdot 6H_2O$ (199 mg), and 1 equiv of phosporic acid dimethyl ester (34 mg) and stirred at room temperature for 12 h. All volatile material was then evaporated under reduced pressure, the residue taken up in acetone (50 mL) and filtered, and the solution layered with light petroleum to gradually yield colorless crystals (193 mg, 74%) of the product **5b**. ^{1}H NMR (500 MHz, d_6-DMSO, 27 °C) δ = 6.09 (s, 1H, pz-H^4), 3.98 (s, 4H, CH_2), 3.66 (d, $^3J_{PH}$ = 11.1 Hz, 6H, OCH_3), 3.05 (m, 4H, CH_2), 2.78 (m, 24H, CH_2), 2.67 (m, 4H, CH_2), 1.03 (s, 24H, CH_3). ^{13}C NMR (126 MHz, d_6-DMSO, 27 °C) δ = 154.0 (pz-C^{3,5}), 99.8 (pz-C^4), 53.8, 53.3, 51.9, 50.0, 47.5, 9.3. ^{31}P NMR (202 MHz, d_6-DMSO, 27 °C) δ = −1.40 (s). IR (KBr) 2981 (m), 2952 (m), 2882 (m), 1474 (m), 1387 (m), 1263 (m), 1223 (m), 1097 (vs), 1052 (s), 1030 (s), 831 (m), 804 (m), 624 (s). MS (ESI) 874 (100, $[Zn_2L^2H_{-1}\{O_2P(OMe)_2\}(ClO_4)]^+$). Elemental analysis calcd (%) for $C_{31}H_{67}Cl_2N_8O_{12}PZn_2$ (976.6) C 38.13, H 6.92, N 11.47; found C 37.55, H 6.78, N 10.86.

Synthesis of $[Zn_2L^4H_{-1}\{O_2P(OMe)_2\}](NO_3)_2$ (6). A solution of L^4 (125 mg, 0.42 mmol) in MeOH (70 mL) was treated with 2 equiv of KO*t*Bu (95 mg), 2 equiv of $Zn(NO_3)_2 \cdot 6H_2O$ (251 mg), and 1 equiv of phosporic acid dimethyl ester (53 mg) and stirred at room temperature for 12 h. All volatile material was then evaporated under reduced pressure, the residue taken up in acetone (50 mL), filtered, and the solution layered with light petroleum to gradually yield colorless crystals (211 mg, 74%) of the product **6**. ^{1}H NMR (500 MHz, d_6-acetone, 27 °C) δ = 6.08 (s, 1H, pz-H^4), 3.81 (d, ^2J = 14.1 Hz, 2H, CH_2), 3.64 (d, ^2J = 14.1 Hz, 2H, CH_2), 3.60 (d, $^3J_{PH}$ = 10.9 Hz, 6H, OMe), 2.87 (m, 2H, N−CH_2), 2.71 (m, 2H, CH_2), 2.51, 2.50 (s, 12H, NMe_2), 1.96 (s, 6H, NMe). ^{13}C NMR (125 MHz, d_6-acetone, 27 °C) δ = 151.7, 102.0, 57.2, 56.0, 53.4, 53.2, 48.0, 44.5, 43.6. ^{31}P NMR (202 MHz, d_6-acetone, 27 °C) δ = 1.11 (s); IR (KBr) 2959 (m), 2909 (m), 2852 (m), 2816 (w), 1482 (s), 1458 (s), 1444 (s), 1385 (s), 1328 (m), 1296 (s), 1237 (s), 1127 (s), 1069 (s), 1047 (s), 1036 (s), 1030 (s), 1016 (m), 967 (m), 831 (m), 809 (m). MS (ESI) 611 (40 $[Zn_2L^4H_{-1}\{O_2P(OMe)_2\}(NO_3)]^+$), 673 (100 $[Zn_2L^4H_{-1}\{O_2P(OMe)_2\}_2]^+$). Elemental analysis calcd (%) for $C_{17}H_{37}N_8O_{10}PZn_2$ (675.3) C 30.24 H 5.52 N 16.59; found C 30.17, H 5.46, N 16.72.

Synthesis of $[Zn_4(L^4H_{-1})_2(OH)_2(NPP)](ClO_4)_2$ (7). A solution of L^4 (53 mg, 0.18 mmol) in MeOH (20 mL) was treated with 1 equiv of KO*t*Bu (20 mg), 2 equiv of $Zn(ClO_4)_2 \cdot 6H_2O$ (134 mg), and 1 equiv of sodium bis(4-nitrophenyl)phosphate (BNPP, 65 mg) and stirred at room temperature for 12 h. After filtration, the solution was slowly allowed to evaporate to gradually yield colorless crystals (31 mg, 27%) of the product **7**. ^{1}H NMR (300 MHz, d_6-DMSO, 20 °C) δ = 8.33 (d,^2J = 9.0 Hz, 2H, Ph^3), 7.61 (d, ^2J = 9.0 Hz, 2H, Ph^2), 6.01 (s, 1H, pz-H^4), 3.78 (d, ^2J = 15.7 Hz, 4H, CH_2), 3.66 (d, ^2J = 15.7 Hz, 4H, CH_2), 2.80 (m, 4H, CH_2), 2.65−2.50 (m, br, 28H, CH_2, CH_3), 2.45 (s, br, 12H, CH_3), 2.25 (s, br, 12H, CH_3). ^{13}C NMR (125 MHz, d_6-DMSO, 27 °C) δ = 151.0 (pz-C^{3,5}), 142.8, 139.5, 125.5, 120.2, 99.2 (pz-C^4), 57.1, 53.9, 52.6, 45.0, 43.8. ^{31}P NMR (121 MHz, d_6-DMSO, 20 °C) δ = 2.15 (s). IR (KBr) 2980 (w), 2900 (w), 2873 (w), 2012 (w), 1591 (m), 1495 (m), 1474 (m), 1338 (s), 1263 (s), 1174 (s), 1096 (vs), 1092 (vs), 999 (s), 970 (m), 895 (m), 625 (m), 581 (w). MS (ESI) 1196 (50, $[Zn_4(L^4H_{-1})_2(OH)_2(NPP)(ClO_4)]^+$).

Kinetic Measurements. The kinetic measurements were performed at 50 °C in buffered solutions of DMSO/water (1:1). MES (2-(*N*-morpholino)ethanesulfonic acid), HEPES (*N*-(2-hydroxyethyl)piperazin-*N*′-2-ethanesulfonic acid), and CHES (2-(*N*-cyclohexylamino)ethanesulfonic acid) were used as buffers. The ionic strength was fixed to 0.1 M with sodium perchlorate. In a typical experiment, 1.5 mL of aqueous buffer solution was mixed with 0.5 mL of complex stock solution (in DMSO) and 0.5 mL of DMSO in a temperature-controlled spectrometric cell. After the mixture was equilibrated for 10 min, 0.5 mL of BNPP stock solution (in DMSO) was added and data collection was started immediately. The cleavage of BNPP was measured by following the increase of the 4-nitrophenolate absorption at 414.5 nm. The activity of the complexes was determined by the method of initial rates. At least two independent measurements were made. Conversion from absorbance to concentration was performed by using the Lambert−Beer law $A = \epsilon_{eff} c$. pH dependency of ϵ_{eff} was determined with 4-nitrophenol in the above solvent mixtures.

ESI-MS Measurements. To a solution of the respective complex in 0.5 mL of methanol was added 1 equiv of dimethylphosphoric acid, sodium bis(*p*-nitrophenyl)phosphate, or a mixture of 1 equiv of sodium bis(*p*-nitrophenyl)phosphate and 1 equiv of concentrated perchloric acid. The solutions were heated for 15 min in a water bath at 45 °C and then injected in the ESI mass spectrometer.

^{31}P NMR Investigations. (i) For the titration experiments, aliquots of a solution of dimethylphosphoric acid (5.6 mM) in a 2:1 d_6-DMSO/aqueous buffer solution (HEPES, pH 8) were added to a solution of **2b** (c_0 = 9.0 mM) or **3** (c_0 = 8.7 mM) in 0.6 mL of the above solvent mixture. The samples were equilibrated for about 6 h before ^{31}P NMR spectra were measured. (ii) Following the synthesis of **7**, a solution of sodium bis(*p*-nitrophenyl)phosphate in DMSO (1.2 μmol, 0.1 mL) was added to a mixture of 1.2 μmol of L^4 and 2.4 μmol of $Zn(ClO_4)_2 \cdot 6H_2O$ in 0.25 mL of DMSO, 0.05 mL of d_6-DMSO, and 0.4 mL of an aqueous buffer solution (HEPES, pH 8) in an NMR tube and kept at 50 °C in a water bath. ^{31}P NMR spectra were measured periodically and evaluated by using the integral ratio of the bis(*p*-nitrophenyl)phosphate peak at −12.5 ppm and the peak of **7** at 1.7 ppm.

pH Potentiometric Titrations. The pH potentiometric titrations were conducted at 25.0 ± 0.1 °C at an ionic strength of 0.2 M (KCl) using a Radiometer PHM 84 pH-meter equipped with a Metrohm 6.0234.100 combined electrode and a Metrohm dosimat 715. Calibration of the electrode and pH-meter was performed using a buffer of potassium biphthalate at pH 4.008, and the concentrations of the HCl 0.2073 M and of the KOH 0.1986 M stock solutions were checked, and a pK_W of 13.765 and an Irving factor of 0.082 were obtained following Gran's method.[40]

(40) Gran, G. *Analyst* **1952**, *77*, 661.

Table 11. Crystal Data and Refinement Details for Complexes **2b**, **3**, **5b**, **6**, and **7**

	$[Zn_2L^2H_{-1}(O_2H_2Me)](ClO_4)_2$ **2b**	$[Zn_2L^3H_{-1}(OH)](ClO_4)_2$ **3**	$[Zn_2L^2H_{-1}(DMP)](ClO_4)_2$ **5b**	$[Zn_2L^4H_{-1}\{O_2P(OMe)_2\}](NO_3)_2$ **6**	$[Zn_4(L^4H_{-1})_2(OH)_2(NPP)](ClO_4)_2 \cdot H_2O \cdot 3MeOH$ **7**
formula	$C_{31}H_{70}Cl_2N_8O_{11}Zn_2$	$C_{29}H_{58}Cl_2N_8O_9Zn_2$	$C_{31}H_{67}Cl_2N_8O_{12}PZn_2$	$C_{17}H_{37}N_8O_{10}PZn_2$	$C_{39}H_{80}Cl_2N_{13}O_{20}PZn_4$
M_r (g/mol)	932.59	864.47	976.54	675.26	1414.51
cryst size (mm)	0.40 × 0.30 × 0.24	0.31 × 0.21 × 0.15	0.50 × 0.30 × 0.20	not determined	not determined
cryst syst	orthorhombic	monoclinic	monoclinic	monoclinic	monoclinic
space group	*Pbca*	$P2_1$	$P2_1/c$	$P2_1/n$	*Cm*
a (Å)	19.1705(10)	9.5207(4)	13.064(3)	11.127(2)	17.586(4)
b (Å)	18.2978(10)	12.1629(5)	13.314(3)	7.9082(16)	14.211(3)
c (Å)	48.448(3)	16.0064(7)	49.813(10)	31.715(6)	12.943(3)
α (deg)	90	90	90	90	90
β (deg)	90	99.780(1)	93.19(3)	95.89(3)	109.96(3)
γ (deg)	90	90	90	90	90
volume (Å^3)	16995(2)	1827(1)	8651(3)	2776(1)	3040(1)
ρ_{calcd} (g/cm^3)	1.458	1.572	1.500	1.616	1.545
Z	16	2	8	4	2
F(000)	7904	908	4112	1400	1468
T (K)	173(2)	190(2)	100(2)	133(2)	133(2)
λ (Å)	0.71073	0.71073	1.54178	0.71073	0.71073
hkl range	0 to 23, 0 to 22, 0 to 60	±13, −17 to 18, 0 to 23	±14, ±14, −55 to 53	−13 to 12, −9 to 8, −37 to 36	±20, ±16, ±15
θ range (deg)	1.35−26.37	1.29−32.03	1.78−60.23	1.89−24.65	1.89−24.69
measd reflns	10 3779	19 758	64 317	12 301	14 092
unique reflns	17 372	10 986	12 679	4603	4786
obsd reflns [$I > 2\sigma(I)$]	13 362	9608	12 375	2952	4427
refined params	1552	662	1350	351	516
restraints	68	1	2606	0	487
resid electron dens (e Å^{-3})	0.821/−0.582	0.897/−0.300	0.571/−0.394	0.516/−0.563	1.155/−0.865
*R*1 [$I > 2\sigma(I)$]	0.047	0.035	0.028	0.039	0.062
wR2 (all data)	0.113	0.086	0.069	0.073	0.149
GOF	1.040	1.022	1.054	1.007	1.034

For the samples, the ligands were pipetted from 8×10^{-3} M stock solutions containing, for L^4 0.021 M HCl, for L^3 0.041 M HCl, and for L^1 0.033 M HCl; zinc(II) was taken from a 0.0979 M $ZnCl_2$ stock solution containing 0.0163 M HCl. Additional HCl was added from the 0.2073 M HCl stock solution, and KCl was taken from a 2 M stock solution. The initial concentrations of the samples were 0.2 M KCl, 3.8 mM ligand L^1, 4.0 ligand L^3, and 3.8 mM ligand L^4 and 0.033 M HCl for L^1, 0.042 M HCl for L^3, and 0.031 M HCl for L^4. The initial $ZnCl_2$ concentration was varied between 2.94 mM, 4.90 mM, or 6.85 mM for L^3 and L^4 and between 2.94 mM and 3.72 mM for L^1.

Titrations of the free ligands were run between pH 2 and 11.5 and, for ligands with added metal solutions, between pH 2 and 11, using the KOH 0.1986 M stock solution. The pH-metric results were utilized to establish the stoichiometry of species and to calculate the stability constants. Calculations were performed with the computer programs SUPERQUAD and PSEQUAD[41], and speciation curves were created with the help of the MEDUSA program.[42]

X-ray Crystallography. Crystal data and experimental conditions are listed in Table 11. Data for **2b** and **3** were collected on a Bruker AXS SMART 1000 CCD diffractometer, for **5b** on a Bruker SMART 6K CCD, and for **6** and **7** with a Stoe image plate IPDS II-system. All structures were solved by direct methods (SHELXS-97)[43] and refined against F^2 using SHELXL-97.[44] The non-hydrogen atoms were refined anisotropically. In general, hydrogen atoms attached to carbon atoms were refined using the riding model, with U_{iso}(H) tied to U_{eq}(C). In the case of **2b** and **3**, many of the H atoms have been located and refined isotropically. Most of the ClO_4^- anions were disordered and refined with distance restraints and restraints for the anisotropic displacement parameters (no restraints in the case of **2b** and **3**). In structure **2b** and **5b**, there are two molecules in the asymmetric unit. In both structures, part of the ligand of one of the molecules is disordered and refined with distance restraints and restraints for the anisotropic displacement parameters. For structure **7**, data of a nonmerohedrally twinned crystal were collected. The twin law 1 0 0 0 −1 0 −0.5025 0 −1 (2-fold rotation about the *a* axis) indicates that the reflections with $h = 2n$ have a contribution of the second twin domain. Additionally, racemic twinning was found. The fractional contributions of the minor domains were refined to 0.16(2), 0.09(2), and 0.02(2). Three MeOH and one H_2O molecules were found and refined without hydrogen atoms. The hydrogen atoms bound to O4 and O5 were refined freely using a distance restraint. An extinction correction was applied for structure **5b**.

Acknowledgment. We sincerely thank the Deutsche Forschungsgemeinschaft (F.M., Project Me1313/5-1), the Fonds der Chemischen Industrie (F.M.), OTKA TS 040685 (E.F.) and COST (Grant D21/0001) for support.

Supporting Information Available: Crystallographic data (in CIF format) for complexes **2b**, **3**, **5b**, **6**, and **7**, pH titration curves, Lineweaver−Burk plots, table of major ESI-MS peaks, and ORTEP plots of **2b**, **3**, **5b**, **6**, and **7**. This material is available free of charge via the Internet at http://pubs.acs.org.

IC035491D

(41) (a) Gans, P.; Sabatini, A.; Vacca, A. *J. Chem. Soc., Dalton Trans.* **1985**, 1195. (b) Zékány, L.; Nagypál, I. In *Computational Methods for the Determination of Stability Constants*; Leggett, D. L., Ed.; Plenum Press: New York, 1985; p 291.

(42) Puigdomenech, I. *MEDUSA and Hydra Software for Chemical Equilibrium Calculations*; Royal Institute of Technology (KTH): Stockholm, Sweden.

(43) Sheldrick, G. M. *Acta Crystallogr. A* **1990**, *46*, 467.

(44) Sheldrick, G. M. *SHELXL: Program for Crystal Structure Refinement*; University of Göttingen: Göttingen, Germany, 1997.